Atmos. Chem. Phys. Discuss., 4, 4131–4189, 2004
www.atmos-chem-phys.org/acpd/4/4131/
SRef-ID: 1680-7375/acpd/2004-4-4131

Atmospheric Chemistry and Physics Discussions

Evaluation of the vertical diffusion coefficients from ERA-40 with ^{222}Rn simulations

D. J. L. Olivié[1, 2], P. F. J. van Velthoven[1], and A. C. M. Beljaars[3]

[1]Royal Netherlands Meteorological Institute, De Bilt, The Netherlands
[2]Eindhoven University of Technology, Eindhoven, The Netherlands
[3]European Centre for Medium-range Weather Forecasts, Reading, UK

Received: 15 June 2004 – Accepted: 15 July 2004 – Published: 3 August 2004

Correspondence to: D. J. L. Olivié (olivie@knmi.nl)

Abstract

Boundary layer turbulence has a profound influence on the distribution of tracers with sources or sinks at the surface. The 40-year ERA-40 meteorological data set of the European Centre for Medium-range Weather Forecasts contains archived vertical diffusion coefficients. We evaluated the use of these archived diffusion coefficients instead of off-line diagnosed coefficients based on other meteorological parameters archived during ERA-40 by investigation of the effect on the distribution of the radioactive tracer ^{222}Rn in the chemistry transport model TM3. In total four different sets of vertical diffusion coefficients are compared: (i) 3-hourly vertical diffusion coefficients archived during the ERA-40 project, (ii) 3-hourly off-line diagnosed coefficients from a non-local scheme based on Holtslag and Boville (1993), Vogelezang and Holtslag (1996), and Beljaars and Viterbo (1999), (iii) 6-hourly coefficients archived during the ERA-40 project, and (iv) 6-hourly off-line diagnosed coefficients based on a local scheme described in Louis (1979) and Louis et al. (1982). The diffusion scheme to diagnose the coefficients off-line in (ii) is similar to the diffusion scheme used during the ERA-40 project (i and iii).

The archived diffusion coefficients from the ERA-40 project which are time-averaged cause stronger mixing than the instantaneous off-line diagnosed diffusion coefficients. This can be partially attributed to the effect of instantaneous versus time-averaged coefficients, as well as to differences in the diffusion schemes. The 3-hourly off-line diagnosis of diffusion coefficients can reproduce quite well the 3-hourly archived diffusion coefficients.

Boundary layer heights are also available for the sets (ii) and (iii). Both were found to be in reasonable agreement with observations of the boundary layer height from Cabauw in the Netherlands and from the FIFE-campaign in the United States.

Simulations of ^{222}Rn with the TM3 model using these four sets of vertical diffusion coefficients are compared to surface measurements of ^{222}Rn in Freiburg, Schauinsland, Cincinnati and Socorro in order to evaluate the effect of these different sets of

ACPD

4, 4131–4189, 2004

Vertical diffusion coefficients from ERA-40

D. J. L. Olivié et al.

diffusion coefficients on the tracer transport. It is found that the daily cycle of the ^{222}Rn concentration is well represented using 3-hourly diffusion coefficients. Comparison with observations of ^{222}Rn data with the station in Schauinsland which is situated on a hill shows that all considered schemes underestimate the amplitude of the daily cycle of the ^{222}Rn concentration in the upper part of the atmospheric boundary layer.

We conclude that the 3-hourly archived diffusion coefficients from ERA-40 are well suited for use in chemistry transport models.

1. Introduction

Boundary layer turbulence is an important transport mechanism in the troposphere (Wang et al., 1999). In the convective or turbulent atmospheric boundary layer (ABL), tracers can be mixed throughout the height range of the ABL in time intervals of tens of minutes. Furthermore all species emitted at the surface must pass through the ABL to reach the free troposphere.

Because turbulence acts on spatial scales that are much smaller than the typical size of the grid cells of global chemistry transport models or global numerical weather prediction models, turbulent diffusion must be parameterised in these models. For parameterisation, often first order closure schemes are applied, where the vertical diffusion coefficients are calculated as a function of the large-scale meteorological variables such as temperature, humidity, surface heat flux, and wind(shear).

Local diffusion schemes often describe the vertical diffusion coefficient as a function of a mixing length scale, the local gradient of the wind, and the virtual temperature (Louis, 1979). However, under convective conditions, when the largest transporting eddies may have sizes similar to the depth of the ABL, local schemes do not perform well (Troen and Mahrt, 1986). A local theory has limitations in the unstable ABL because the characteristics of the large eddies are not properly taken into account.

Non-local ABL schemes contain a term that describes counter gradient transport by the large eddies (Troen and Mahrt, 1986), and usually prescribe the shape of the

ACPD
4, 4131–4189, 2004

vertical profile of the diffusion coefficient. Holtslag and Boville (1993) have compared the effect of using a local and non-local ABL scheme in a global climate model, the Community Climate Model, Version2 (CCM2). The vertical exchange of moisture appeared to be much more pronounced with the non-local scheme than with the local scheme. Holtslag et al. (1995) compared the results of a local and a non-local scheme for vertical diffusion with observations at the 200-m tower at Cabauw, the Netherlands. They also found that the non-local scheme transports moisture away from the surface more rapidly than the local scheme, and deposits the moisture at higher levels. The local scheme tended to saturate the lowest model levels unrealistically in comparison with the observations. Wang et al. (1999) have implemented the scheme from Holtslag and Boville (1993) into a tropospheric chemistry model. The scheme includes the calculation of atmospheric radiative transfer, surface energy balance, and land surface temperature. They compared the use of that non-local diffusion scheme with a local diffusion scheme by verifying it against measurements of ^{222}Rn and CH_4. They found that using the non-local scheme, more O_3 is transported from the middle-troposphere down to the surface, while more CO is pumped up from the surface into the middle troposphere.

Chemistry transport models that are off-line coupled to a climate or weather forecast model, have to diagnose turbulent diffusion based on frequently (e.g. 6-hourly) archived meteorological data. Rasch et al. (1997) have studied the effect of using off-line diagnosed instead of archived (time-averaged or instantaneous) meteorological parameters to describe the sub-grid scale vertical transport by turbulent diffusion and convection. They show that the errors in off-line model simulations (compared to the on-line situations) can be made small when the sampling interval is 6 hours or less. In the past, meteorological fields describing small-scale transport like convection or boundary layer turbulence were often not archived. One of the first to use archived sub-grid convective mass fluxes was Allen et al. (1996). They used archived convective mass fluxes and detrainments, as well as the ABL heights.

The global chemistry transport model TM3 uses meteorological data from the Eu-

ACPD
4, 4131–4189, 2004

ropean Centre for Medium-range Weather Forecasts (ECWMF). Until now, two off-line vertical diffusion schemes have been used in the TM3-model: one based on Louis (1979) and Louis et al. (1982), and one based on a combination of Holtslag and Boville (1993), Vogelezang and Holtslag (1996) and Beljaars and Viterbo (1999). In the more recent ERA-40 data set (Simmons and Gibson, 2000), vertical diffusion coefficients for heat are archived. It is one of the first long-term meteorological data sets where these coefficients have been archived. The archived coefficients are available as 3- or 6-hourly averaged values. In this study, we will investigate how well these different sets of diffusion coefficients represent turbulent tracer transport in the TM3-model. The 3-hourly off-line scheme (Holtslag and Boville, 1993; Vogelezang and Holtslag, 1996; Beljaars and Viterbo, 1999) is currently most used in the TM3 model. We will compare it with the 3-hourly archived data. The 6-hourly off-line scheme (Louis, 1979; Louis et al., 1982) was until recently used in the TM3 model for various studies: Dentener et al. (2003a) used meteorological data from the ERA-15 project (which does not contain 3-hourly surface latent heat fluxes) and the 6-hourly off-line scheme (Louis, 1979; Louis et al., 1982). Their results will be sensitive to the description of the diffusion. Therefore it is interesting to study the effect of archived versus off-line diagnosed coefficients, the effect of 3-hourly versus 6-hourly diffusion coefficients, the effect of time-averaged versus instantaneous coefficients, and the effect of differences in the schemes.

^{222}Rn is an excellent tracer to study the transport of tracers on short time scales (hours to weeks) because it has an almost uniform emission rate over land and is only lost through radioactive decay with an e-folding lifetime of about 5.5 days (Dentener et al., 1999). Therefore ^{222}Rn has been used extensively to evaluate parameterisations of convective transport (Mahowald et al., 1997; Allen et al., 1996; Feichter and Crutzen, 1990; Jacob and Prather, 1990) and ABL diffusion (Stockwell and Chipperfield, 1999; Stockwell et al., 1998; Jacob et al., 1997; Lee and Larsen, 1997; Mahowald et al., 1997) in atmospheric models. We will use measurements of ^{222}Rn concentrations at the surface in continental stations at Freiburg, Schauinsland, Socorro and Cincinnati for evaluating the model simulations.

ACPD
4, 4131–4189, 2004

In Sect. 2, we describe the TM3 model and the diffusion schemes that generate the vertical diffusion coefficients. We compare the vertical diffusion coefficients from the different schemes. In Sect. 3 we compare the ABL height from the non-local schemes with ABL height measurements, and compare the modelled ^{222}Rn concentration with surface measurements. In Sect. 4, we will discuss the results and formulate the conclusions.

2. The TM3 model

2.1. Vertical diffusion

The vertical diffusion of tracers in the TM3 model is described with a first order closure. The net turbulent tracer flux $\overline{w'\chi'}$ is expressed as

$$-\overline{w'\chi'} = K_h \frac{\partial \chi}{\partial z}, \quad (1)$$

where K_h is the vertical diffusion coefficient for heat, w the vertical velocity, χ the concentration of some tracer, and z the height above the surface. It is assumed that the vertical diffusion coefficient for tracers is equal to the vertical diffusion coefficient for heat.

Different sets of vertical diffusion coefficients are used in the TM3 model. We will briefly describe the schemes that are used to calculate these data sets.

2.1.1. The ERA-40 3-hourly and 6-hourly diffusion coefficients

The scheme as it is used in the ERA-40 project is described in the documentation of the cycle CY23r4 of the ECMWF model, see http://www.ecmwf.int/research/ifsdocs/CY23r4/. It is a non-local scheme. The coefficients for vertical diffusion of heat were stored during the ERA-40 project as 6-hourly or 3-hourly averaged values.

ACPD
4, 4131–4189, 2004

If the surface layer is unstable ($(\overline{w'\theta'_v})_0>0$), then a method according to Troen and Mahrt (1986) is applied. $(\overline{w'\theta'_v})_0$ is the virtual heat flux at the surface. This method determines the ABL height using a parcel method where the parcel is lifted from the minimum virtual temperature, rather than from the surface. The coefficient for the excess of the parcel temperature is reduced from 6.5 (Troen and Mahrt, 1986) or 8.5 (Holtslag and Boville, 1993) to 2. In the ABL, the vertical profile of diffusion coefficients is predefined (Troen and Mahrt, 1986)

$$K_h = \kappa\, w_h\, z \left(1 - \frac{z}{h}\right)^2, \tag{2}$$

where w_h is a turbulent velocity scale and κ=0.4 the Von Karman constant.

At the top of the ABL, there is an explicit entrainment formulation in the capping inversion. The virtual heat flux is taken proportional to the surface virtual heat flux

$$(\overline{w'\theta'_v})_h = -C\,(\overline{w'\theta'_v})_0, \tag{3}$$

with C=0.2 and θ_v the virtual potential temperature. Knowing the flux, the diffusion coefficient can be expressed as

$$K_h = C\,\frac{(\overline{w'\theta'_v})_0}{\frac{\partial\theta_v}{\partial z}}, \tag{4}$$

where $\frac{\partial\theta_v}{\partial z}$ is the virtual potential temperature gradient in the inversion layer.

If the surface layer is stable ($(\overline{w'\theta'_v})_0<0$), the diffusion coefficients are determined in the following way. The gradient Richardson number Ri is defined as

$$Ri = \frac{g}{\theta}\,\frac{\frac{\partial\theta}{\partial z}}{\left|\frac{\partial \mathbf{v}}{\partial z}\right|^2}, \tag{5}$$

ACPD
4, 4131–4189, 2004

where $\boldsymbol{v}$ is the horizontal wind velocity. When the atmosphere is locally unstable ($Ri<0$) then

$$K_h = \frac{l_h^2}{\Phi_m \Phi_h} \left| \frac{\partial \boldsymbol{v}}{\partial z} \right|, \tag{6}$$

where

$$\Phi_m(\zeta) = (1 - 16\,\zeta)^{-\frac{1}{4}}, \tag{7}$$

and where

$$\Phi_h(\zeta) = (1 - 16\,\zeta)^{-\frac{1}{2}}, \tag{8}$$

where ζ is taken equal to Ri. The mixing length is calculated according to

$$\frac{1}{l_h} = \frac{1}{\kappa\, z} + \frac{1}{\lambda_h}. \tag{9}$$

The asymptotic mixing length is defined as

$$\lambda_h = 30 + \frac{120}{1 + \left(\frac{z}{4000}\right)^2}. \tag{10}$$

When the atmosphere is locally stable ($Ri>0$), ζ is read from a table ($\zeta=\zeta(Ri)$). The diffusion coefficients are calculated with

$$K_h = l_h^2 \left| \frac{\partial \boldsymbol{v}}{\partial z} \right| F_h(Ri), \tag{11}$$

where the stability function $F_h(Ri)$ is a revised function of the Louis et al. (1982) function (Beljaars and Viterbo, 1999)

$$F_h(Ri) = \frac{1}{1 + 2\,b\,Ri\sqrt{1 + d\,Ri}}, \tag{12}$$

ACPD
4, 4131–4189, 2004

where b=5 and d=1. This formulation has less discrepancy between momentum and heat diffusion: the ratio of momentum and heat diffusion is reduced (Viterbo et al., 1999). The formulation of K_h in case of a stable surface layer also applies to the formulation of K_h above the ABL in case of an unstable surface layer.

The calculation of the atmospheric boundary layer height stored during the ERA-40 project is also described in the information about the cycle CY23r4. As well in the stable, in the neutral, as in the unstable case, a parcel lifting method proposed by Troen and Mahrt (1986) is used. They use a critical bulk Richardson number Ri_b=0.25. The bulk Richardson number is based on the difference between quantities at the level of interest and the lowest model level. This ABL height is available every 3 and 6 h and represents an instantaneous value. We only studied the 6-hourly values. A plot of the mixing length and asymptotic mixing length for heat in the different schemes is shown in Fig. 1. We will refer to these 3-hourly diffusion coefficients as E3, and to these 6-hourly diffusion coefficients and 6-hourly ABL heights as E6.

2.1.2. The TM3 off-line 3-hourly and 6-hourly diffusion coefficients

The first set of off-line diagnosed diffusion coefficients in TM3 is calculated with a scheme that is rather similar to the above-described scheme. It is a non-local scheme based on Holtslag and Boville (1993), Vogelezang and Holtslag (1996), and Beljaars and Viterbo (1999). The diffusion coefficients are calculated every 3 h, based on 3-hourly latent and sensible heat fluxes, and 6-hourly fields of wind, temperature, humidity and geopotential height. It has been implemented and tested in the TM3 model (Jeuken, 2000; Jeuken et al., 2001). The calculated K_h values are instantaneous values.

Although the scheme is rather similar to the aforementioned E3/E6 scheme, there are some differences. (i) A bulk Richardson criterion instead of a parcel ascent method is used to determine the height of the ABL. (ii) There is no entrainment formulation at the top of the ABL. (iii) The temperature excess of the large eddies under convective conditions is larger. (iv) The prescribed profile of the asymptotic mixing length is

ACPD
4, 4131–4189, 2004

different. (v) The stability functions are different.

If the surface layer is unstable ($(\overline{w'\theta'_v})_0>0$), a prescribed profile of the vertical diffusion coefficients as in Eq. 2 is used. According to Vogelezang and Holtslag (1996) the ABL height h is the layer where the bulk Richardson number

$$Ri_b = \frac{\frac{g}{\theta_{vs}}(\theta_{vh} - \theta_{vs})(h - z_s)}{|\boldsymbol{v}_h - \boldsymbol{v}_s|^2 + b\,u_*^2} \tag{13}$$

reaches a critical value Ri_b=0.3. (In Vogelezang and Holtslag (1996), the critical value is Ri_b=0.25.) The index s refers to values in the lowest model layer, the index h refers to values at the top of the ABL. u_* is the friction velocity. The value for b=100. The exact ABL height is calculated by linear interpolation. The temperature excess under convective conditions is calculated using a coefficient with value 8.5 (instead of 2 in the E3/E6 case).

If the surface layer is stable ($(\overline{w'\theta'_v})_0<0$), the diffusion coefficients are calculated with Eq. (11). When the atmosphere is locally stable ($Ri>0$), we take

$$F_h(Ri) = \frac{1}{1 + 10\,Ri\sqrt{1 + Ri}}, \tag{14}$$

while when the atmosphere is locally unstable ($Ri>0$) we take

$$F_h(Ri) = 1. \tag{15}$$

Above the ABL, a formulation according to the Louis (1979) scheme is used. In the free atmosphere the stability functions in the unstable case ($Ri<0$) (Williamson et al., 1987; Holtslag and Boville, 1993) is

$$F_h(Ri) = \sqrt{1 - 18\,Ri}, \tag{16}$$

and in the stable case ($Ri>0$) (Holtslag and Boville, 1993)

$$F_h(Ri) = \frac{1}{1 + 10\,Ri(1 + 8\,Ri)}. \tag{17}$$

ACPD
4, 4131–4189, 2004

The asymptotic mixing length in this scheme is defined as

$$\lambda_h = \begin{cases} 300 & \text{if} \quad z < 1000 \text{ m} \\ 30 + 270 \exp\left(1 - \frac{z}{1000}\right) & \text{if} \quad z \geq 1000 \text{ m}, \end{cases} \tag{18}$$

and shown in Fig. 1. In contrast to Holtslag and Boville (1993) and Wang et al. (1999), there is no counter gradient term in the implementation as it is used here.

We will refer to the diffusion coefficients calculated with this diffusion scheme as H3.

The second set of diffusion coefficients which are off-line diagnosed in TM3 is based on a local diffusion scheme described in Louis (1979) and Louis et al. (1982). These fields of vertical diffusion coefficients are calculated every 6 h, based on 6-hourly fields of wind, temperature, humidity and geopotential height. The vertical diffusion coefficients are expressed as in Eq. (11). The stability function $F_h(Ri)$ in the stable case ($Ri>0$) is

$$F_h(Ri) = \frac{1}{1 + 3\,b\,Ri\sqrt{1 + d\,Ri}}, \tag{19}$$

where b=5 and d=5, and in the unstable case ($Ri<0$)

$$F_h(Ri) = 1 - \frac{3\,b\,Ri}{1 + 3\,b\,c\,l_h^2\sqrt{-\frac{Ri}{2}\left[\frac{\left(1+\frac{\Delta z}{z}\right)^{\frac{1}{3}}-1}{\Delta z}\right]^3}}, \tag{20}$$

where c=5. The asymptotic mixing length λ_h is taken to be 450 m.

We will refer to this diffusion scheme as L6.

2.2. ^{222}Rn emission

^{222}Rn is an excellent tracer for evaluating transport parameterisations (Dentener et al., 1999; Allen et al., 1996; Balkanski and Jacob, 1990; Feichter and Crutzen, 1990; Jacob and Prather, 1990; Kritz et al., 1990; Brost and Chatfield, 1989; Polian et al., 1986).

ACPD
4, 4131–4189, 2004

^{222}Rn is emitted at a relatively uniform rate from the soil on the continents. It is relatively insoluble in water, inert and not efficiently removed by rain. It has a mean e-folding lifetime of about 5.5 days due to radioactive decay. It is generally accepted that the average flux from the soil lies somewhere between 0.8 and 1.3 atoms cm^{-2} s^{-1} (Liu et al., 1984; Turekian et al., 1977; Wilkening and Clements, 1975). Oceans are also a source for ^{222}Rn. However, the mean oceanic flux is estimated to be 100 times weaker than the continental source (Lambert et al., 1982; Broecker et al., 1967). The fact that ^{222}Rn has a lifetime and source characteristics that are similar to the lifetime and source characteristics of air pollutants such as NO, NO_2, propane, butane and other moderately reactive hydrocarbons, makes it interesting for evaluation of transport parameterisations.

We adopted the emission scenario recommended by WCRP (Jacob et al., 1997): land emission between 60° S and 60° N is 1 atoms cm^{-2} s^{-1}; land emission between 70° S and 60° S and between 60° N and 70° N is 0.005 atoms cm^{-2} s^{-1}; oceanic emission between 70° S and 70° N is 0.005 atoms cm^{-2} s^{-1}. This leads to a global ^{222}Rn emission of 16 kg per year. We did not account for any regional or temporal variation in the emission rate. A slightly different emission scenario has been proposed by Conen and Robertson (2002), which includes a linearly decreasing emission north of 30° N. We did not use this scenario.

2.3. The TM3 chemical transport model

The chemical transport model TM3 (Tracer Model Version 3) is a global atmospheric model which is used to evaluate the atmospheric composition and changes herein caused by natural and anthropogenic changes (Dentener et al., 2003a,b; Lelieveld and Dentener, 2000; Meijer et al., 2000; Dentener et al., 1999; Houweling et al., 1998; van Velthoven and Kelder, 1996). For this study, the TM3 model has a regular longitude-latitude grid and hybrid σ-pressure levels up to 10 hPa. The model is used with a 2.5°×2.5° grid and 31 layers. The lowest layer has a thickness of about 60 m, the

ACPD
4, 4131–4189, 2004

second layer of about 150 m.

The meteorological input data from ERA-40 is available for 1957 to 2002. For dynamics calculations ERA-40 used a spectral truncation of T159. The physical calculations were done on a reduced Gaussian grid of 160 nodes. In the vertical, 60 hybrid σ-pressure levels (Simmons and Burridge, 1981) were used, reaching up to 0.1 hPa. To be used in the TM3 model, the meteorological data is interpolated or averaged to the desired TM3 grid cells (Bregman et al., 2003). For advection of the tracers, the model uses the slopes scheme developed by Russel and Lerner (Russell and Lerner, 1981). To describe the effect of convective transport on the tracer concentration, we used the archived convective mass fluxes from the ERA-40 data set (Olivié et al., 2004). The convection scheme is based on Tiedtke (1989), but has since then evolved (Gregory et al., 2000; Nordeng, 1994).

The four sets of vertical diffusion coefficients (E3, H3, E6, and L6) are applied in the model by converting the vertical diffusion coefficients into equal upward and downward vertical air mass fluxes. These air mass fluxes are combined with the vertical convective mass fluxes from the convection parameterisation to calculate the sub-gridscale vertical tracer transport with an implicit scheme. This allows the timesteps to be rather big, without introducing stability problems. In the case of very large timesteps, the effect of the scheme is that it pushes the tracer distribution to its equilibrium distribution. In this study, we used a timestep of 1 hour for the small-scale vertical transport.

We have performed model simulations with the chemistry transport model TM3 separately for each of the available sets of vertical diffusion coefficients. To allow comparisons with ^{222}Rn measurements, we made model simulations from November 1958 until February 1963, and from November 1992 until December 1993. We used 5 model setups: (E3) using 3-hourly averaged fields from the scheme in Sect. 2.1.1, (H3) using 3-hourly instantaneous fields from the first scheme in Sect. 2.1.2; (E6) as E3 but with 6-hourly averaged fields, (L6) using 6-hourly instantaneous fields according to the second scheme in Sect. 2.1.2, and (N) using no diffusion. Table 1 gives an overview of the different model simulations.

ACPD
4, 4131–4189, 2004

For the comparison of the ABL height, we compared the ABL height of the H3 scheme described in Sect. 2.1.2 and the ABL height as it is stored in the ERA-40 data (E6, see Sect. 2.1.1). The ABL height from the H3 case is available every 3 h. The ABL height calculated during the ERA-40 project (E6) is available every 6 h. There are no ABL heights available for the L6 scheme: because the L6 scheme is a local scheme, there is no explicit ABL height in the L6 scheme. For the comparison of the ABL height we used data from the years 1987, 1989, and 1996. In Table 1, one can see an overview of the properties of the two sets of ABL heights.

2.4. Comparison of the diffusion coefficients

The zonal and monthly mean diffusion coefficients from the E3/E6 scheme, the H3 scheme, and the L6 scheme are shown in Figs. 2 and 3 for January and July 1993. In Fig. 2, the diffusion coefficients are given as a function of pressure. High values below 600 hPa correspond to the presence of an ABL, a local maximum around 300 hPa corresponds to strong vertical wind gradients in the upper troposphere. The summer winter variations are captured by all the schemes. In Fig. 3 where the profiles for the lowest 3 km are given, one sees that the value of the diffusion coefficients in the lowest two or three layers are almost identical.

However, there are also differences between the diffusion coefficients of the schemes. One sees in Figs. 2 and 3 that the L6 diffusion is in general stronger than the E3/E6 and H3 diffusion. The largest relative differences can be found above the ABL. In the free atmosphere the L6 diffusion coefficients are 2 to 3 orders of magnitude larger than the H3 diffusion coefficients. This is mainly due to the difference in the asymptotic mixing length: 450 m in the L6 case, 30 m in the H3 case. The E3/E6 coefficients in the free atmosphere are located between the L6 and H3 case. They have the tendency to correspond at lower altitudes in the free troposphere with L6, while higher up they tend to the H3 case.

Other differences between the H3 and E3/E6 case, are due to differences in the stability functions. The stability functions when the atmosphere is locally stable are

ACPD
4, 4131–4189, 2004

quite similar. However, when the atmosphere is locally unstable, the values can be quite different: above the ABL, the stability function for the H3 case is larger than for the E6/E3 case, and in the stable boundary layer, the stability function for the H3 case is smaller than for the E6/E3 case.

One should note that the shape of the profile for the H3 and E3/E6 case in the ABL is very similar. These off-line diagnosed coefficients (H3) and archived coefficients (E3/E6) are based on similar schemes.

3. Evaluation of the boundary layer height and simulated ^{222}Rn concentration

3.1. Evaluation of the model simulated atmospheric boundary layer height

We compared the 6-hourly ABL height from the ERA-40 data (E6), and the 3-hourly ABL height diagnosed in the H3-scheme with measured ABL heights. We used measurements of ABL heights at Cabauw in the Netherlands during some days in the summer of 1996, and measurements made during the FIFE campaign during several days in the summer of 1987 and 1989 in the United States (US). For Cabauw, 12 days are available, for the FIFE campaign 22 days are available.

The ABL height in Cabauw (52.0° N, 4.9° E) is derived from measurements with a wind profiler during the day, and a SODAR (Sound Doppler Acoustic Radar) during the night. The wind profiler is a pulsed Doppler radar. The strength of the echo from the radar pulse depends on the turbulence intensity. In the clear air case (no clouds or rain drops), the strength of the echo is directly proportional to the eddy dissipation velocity, and ABL heights can be derived from it in a straightforward manner. The profiles have a resolution of 100 m below 2 km (to detect ABL heights below 2 km), and 400 m above (to detect ABL heights larger than 2 km). The SODAR measures wind velocities and wind directions between 20 and 500 m by emitting sound pulses and measuring the reflection of this pulse by the atmosphere.

The field experiments of the First ISLSCP Field Experiment (FIFE) (Sellers et al.,

ACPD
4, 4131–4189, 2004

1988) were performed in 1987 and 1989 near Manhattan (39.1° N, 96.5° E), Kansas, US. The measurements of ABL height were done with a Volume Imaging LIDAR (Eloranta, 1994). The Volume Imaging LIDAR is an elastic backscatter LIDAR which uses atmospheric light-scattering particles as tracers. The volume imaging LIDAR measures the radial component of the air velocity. It works at a wavelength of 106.4 nm.

The calculated and measured ABL heights during the FIFE campaign are shown in Fig. 4, for Cabauw they are shown in Fig. 5. The maximum value of the height of the ABL is quite well represented both for the E6 and H3 case. Also the time of strongest growth and decrease is well represented. In Cabauw, during three nights the measured ABL height is considerably smaller than the modelled values. On 15 August, the modelled ABL height is much smaller than the measured ABL height. In Fig. 6 scatter plots of the available data are shown. To get a continuous modelled ABL height as a function of time, we interpolated the calculated ABL height. For large timesteps, this can lead to large deviations. The correlation of the observed with the modelled ABL heights is given in Table 2. We see that the quality of the ERA-40 ABL height and the H3 ABL height are similar in the comparison with data from Cabauw: for both schemes, the ABL height in the afternoon falls off in the models sometimes too fast, and is at night sometimes too high, leading to a rather flat correlation curve. In the comparison with data from the FIFE campaign, the H3 ABL height is performing better than the ABL height from ERA-40 (E6). This supports the conclusion that a 6-hourly resolution is not enough to describe the boundary layer evolution. The ERA-40 ABL height seems to be slightly too large.

In assessing the deficiencies, one must keep in mind that the ABL height measurements are made at a point, while the modelled ABL height is representative for a larger area (2.5°×2.5°). This can explain part of the discrepancy. This representation error might be considerable in the case of the measurements made at Cabauw. Due too a strong heterogeneity of the surface, the latent surface heat flux in the model for the grid box where Cabauw is in, maybe does not correspond with the local heat flux at Cabauw. This gridbox contains part of the North Sea and parts of the Ijsselmeer which

ACPD
4, 4131–4189, 2004

might decrease the mean surface latent heat flux in the grid box.

The poor agreement in the afternoon in Cabauw during June 7th and 8th might be caused by the presence of clouds at the top of the boundary layer in the afternoon. The results of the ABL height measurement are not accurate in the presence of clouds. These measurements lead to the poor agreement in the lower right corner of the scatter plot in Cabauw in Fig. 6.

Only measurements on a limited number of days during summer in two mid-latitude locations are evaluated here. The comparison of the ABL height is hampered by the fact that measurements of ABL height in the presence of clouds are difficult.

In general, the low time resolution of the ABL height in the model (especially E6) will degrade its usefulness for the description of the time evolution of the ABL. The meteorological fields are available for fixed GMT, not for fixed LT. This can affect the quality of the reproduction of the ABL height evolution depending on longitude and latitude. There will be longitudes where only one model value is during daytime for 6-hourly fine resolution. In spite of the aforementioned deficiencies, we can conclude that the ABL heights as calculated during the ERA-40 project (E6) and with the H3 scheme, agree reasonably with the measurements.

3.2. Comparison with ^{222}Rn measurements in Freiburg and Schauinsland

We compared the simulated ^{222}Rn concentrations from the TM3 model with surface observations from Freiburg and Schauinsland in Germany, and Cincinnati and Socorro in the US. These are all continental mid-latitudinal surface stations, showing a strong variation in the measured ^{222}Rn concentration during the day as a result of the distinct daily cycle in the ABL diffusion.

We used hourly measurements of ^{222}Rn at Freiburg and Schauinsland (both at 48° N, 8° E) for the year 1993. These data have been used in a study by Dentener et al. (1999). Freiburg and Schauinsland are located at heights of 300 and 1200 m above sea level, respectively. Schauinsland is located approximately 12 km south of Freiburg. For comparison with these observations, we performed model simulations from November

ACPD
4, 4131–4189, 2004

1992 until December 1993. November and December 1992 are included as a spin up period. The analysis is restricted to the year 1993. For this period we performed 5 simulations, each with different vertical diffusion coefficients, as listed in Table 1.

3.2.1. Seasonal cycle of the modelled and measured ^{222}Rn concentration

The monthly mean values of the ^{222}Rn concentration, the correlation of the modelled with the observed daily mean values, and the correlation of the modelled with the observed deviation from the mean daily value for the year 1993 in Freiburg and Schauinsland are shown in Fig. 7. Table 3 gives the 1993 yearly mean ^{222}Rn concentration. All schemes reproduce the monthly mean values quite well, both in Freiburg and in Schauinsland. In Freiburg, the spread in mean concentration between the different diffusion schemes is about 20%. The L6 scheme results in the highest mean concentrations, the E6 scheme in the lowest mean concentrations. The E3 case gives almost similar results as the E6 scheme. In Schauinsland, the spread in the modelled result is much smaller (except in February), but the correspondence with the measurements is smaller. For both stations, the correlation of the modelled with the observed mean daily values is higher than the correlation of the modelled with the observed hourly values (not shown), and the correlation of the modelled with the observed deviation from the mean daily value is smallest. There is also a remarkable difference between the correlation of the modelled with the observed deviation between the E6 and the E3 case, as well in Freiburg as Schauinsland. Table 4 gives the correlations between the observed and modelled ^{222}Rn concentration.

All the aforementioned deficiencies indicate that the daily cycle is hard to reproduce. We will now investigate this in more detail.

3.2.2. Daily cycle

The mean daily cycle of the ^{222}Rn concentration in Freiburg and Schauinsland for December, January and February (DJF) and for June, July and August (JJA) are shown

ACPD
4, 4131–4189, 2004

in Fig. 8. In Freiburg, the daily cycle of the L6 case is largest. The daily cycle of the H3 case corresponds best with the observations. The E3 and E6 cases are very similar, except for the periods 06:00–09:00 h and 15:00–21:00 h (only in DJF) where the E6 case results in lower ^{222}Rn values. For all schemes the daytime concentrations are almost the same in JJA, while differences persist in DJF. The early morning value in JJA for the E3, H3, and E6 case correspond very well with the observed values. However during daytime there is some deviation.

The daily cycle in the model simulations in Schauinsland is not as strong as in the measurements. The deviation is quite large in DJF. In JJA, the simulations reproduce an increase in the concentration in the morning, but not large enough. The schemes differ in the time-positioning of this increase. Notice however that also in Schauinsland, the early morning concentration in JJA is well reproduced.

In Fig. 8, one can clearly identify the times when the meteorological fields are updated. We also do not reproduce high frequency variability of the daily cycle, especially in JJA where the influence of ABL turbulence and convection on the tracer concentration in the lower troposphere can be strong. The second maximum in the measurements in JJA in Schauinsland is clearly not present in the model simulations (except for the H3 case). This can not be expected anyway due to the coarse time and spatial resolution.

3.2.3. Seasonal variation of daily minimum, maximum and amplitude of ^{222}Rn concentration

The daily minimum, daily maximum and daily amplitude of the ^{222}Rn concentration are closely related to the daily cycle of the ABL turbulence. In Fig. 9 the monthly mean value of the daily minimum, maximum and amplitude are shown. It can be seen that in Freiburg these values correspond quite well with the measurements. The amplitude is slightly overestimated by the L6 scheme, while it is underestimated by the E3, H3 and E6 scheme. At the same time the correlation (not shown) of the modelled with the observed daily amplitude is considerably smaller than the correlation of the modelled

ACPD
4, 4131–4189, 2004

with the observed daily minimum or daily maximum. In Schauinsland, we see that the minimum values in the model are in general higher than the observed minimum values, that the maximum values are in general smaller than the observed values, and that the modelled amplitude is therefore much smaller than the observed amplitude. The amplitude in the L6 case is largest. In Schauinsland, the variation between the schemes is much smaller than in Freiburg.

3.2.4. Timeshift

The diffusive and convective mass fluxes are updated in the TM3 model every 3 or 6 h. The updates have a strong influence on the modelled ^{222}Rn distribution (see Fig. 8). The simulations show that the more frequent the updates are, the better the correspondence with the measurements is: E3 performs better than E6, H3 performs better than L6.

Averaging of diffusion coefficients over a certain time interval leads to a strong influence of the large diffusion coefficients during a part of this interval on the time-averaged diffusion coefficient, and thus on the concentration and transport in the tracer transport model. If one compares the E6 and E3 case, it shows up as an earlier start and a sustained prolongation of the low daytime ^{222}Rn values in Freiburg (see again Fig. 8). Using instantaneous diffusion coefficients can maximally lead to a timeshift of half the timestep. Using a time-averaged value can lead in the extreme case to a timeshift of almost the whole timestep. This has a considerable influence in case of timesteps of 6 h. This might also play an important role for other tracers than ^{222}Rn where chemistry and dry deposition come into play.

We have investigated this effect by correlating the modelled morning concentrations (from 00:00 until 12:00 GMT) with time-shifted observed concentrations. The correlation as a function of the applied timeshift is shown in Fig. 10 for the periods March–April–May (MAM) and JJA. The strongest timeshift is found for the E6 and E3 case (E6 stronger than E3), which both use time-averaged diffusion coefficients. The timeshift is smallest for the L6 and H3 case (instantaneous values). With an applied timeshift

ACPD
4, 4131–4189, 2004

of 3 h for the E3 case, and up to 4 or 5 h in the E6 case, the E3 and E6 case perform equally good (JJA) or better (MAM) than the H3 scheme.

We have also correlated the modelled afternoon concentrations (from 12:00 until 24:00) with time-shifted observed concentrations. This resulted in slightly smaller timeshifts with the highest correlation for shifts back in time in the E6 and E3 case (corresponding to persistent low ^{222}Rn concentrations at the end of the day).

3.2.5. Ratio between ^{222}Rn concentration in Freiburg and Schauinsland

Because the stations at Freiburg and Schauinsland are close to each other (12 km), and the station at Schauinsland lies on a hill 900 m higher than Freiburg, these stations are quite well suited to study vertical concentration gradients in the model. Ideally we would prefer to use co-located observations, however tower measurements were not available to us. We would certainly advise to make such measurements in the future. We calculated the correlation of the observed with the modelled ratio of the ^{222}Rn concentration in Freiburg and the ^{222}Rn concentration in Schauinsland. In Fig. 11 and Table 5 the correlation between the ratio in the model and the ratio in the measurements is given.

Because we expect a strong dependence of the aforementioned ratio on the ABL height, we have grouped the measured and modelled ratios as a function of the height of the ABL. For the height of the ABL we took the values of the ABL height as they are calculated in the H3 scheme. These are calculated every 3 h and correspond well with observations (see Sect. 3.1). Because the ^{222}Rn data are available hourly, we interpolated the ABL to an hourly resolution. We also tried this with the 6-hourly ABL heights from the ERA-40 data set. We noticed however that this gave more noisy relationships (as expected due to the coarser time resolution of the ABL height).

In Fig. 11 one can observe that the fraction becomes smaller as a function of the height of the ABL top. We would expect a large drop in the ratio when the ABL height reaches higher than the station in Schauinsland. One expects hyperbolic behaviour for ABL heights below 800–1000 m, and a sharp drop in the ratio around 800–1000 m. We

ACPD
4, 4131–4189, 2004

see however that as well for the observed ratio as for the modelled ratio, the transition point is around 500 m, and not around 800–1000 m. This can be related to the course vertical resolution, the large scatter of the data, and the use of a modelled ABL height to deduce these curves. The L6 scheme shows the strongest correspondence with the measurement, the E6 scheme shows the worst correspondence. The observed ratio is in general higher than the modelled ratio. This partially results from lower concentrations in Freiburg and higher concentrations (DJF) in Schauinsland. The curves seem to suggest that the vertical transport is stronger in the model than in the observations. This might however also be influenced by local geographical influences on the atmospheric mixing.

3.3. Comparison with ^{222}Rn measurements in Cincinnati and Socorro

We used monthly mean ^{222}Rn measurements made in Cincinnati (40° N, 84° W) at 08:00 and 15:00 LT from January 1959 until February 1963 (Gold et al., 1964), and monthly mean daily cycles of the ^{222}Rn concentration in Socorro (34° N, 107° W) (Wilkening, 1959). The measurements at Socorro were made between 1951 and 1957. Although the measurements were not continuous (only 692 days were sampled during this period), they might give a good indication of the average monthly mean daily cycle of the ^{222}Rn concentration in Socorro. For comparison with these observations, we analyzed the period from January 1959 until February 1963 and used November and December 1958 as a spin up period. For this period we performed 3 simulations: using 6-hourly L6 data, using 3-hourly H3 data and using 6-hourly E6 data (for the meaning of the code, see Table 1).

The measurements in Cincinnati were in the past extensively used in tracer transport models in a climatological sense. The ERA-40 reanalysis which starts from the year 1957 now allows a month to month comparison of these measurements. However, the observational data for April and May 1959 are lacking.

Figure 12 gives the observed and modelled monthly mean surface concentration in Cincinnati for 08:00 and 15:00 LT from January 1959 until February 1963. The

ACPD
4, 4131–4189, 2004

seasonal variation in the observations seems to be much larger than in the model. Gold et al. (1964) attribute this to freezing minimizing the emission in winter, and to an increasing emanation rate of ^{222}Rn due to the decrease of the moisture content of the soil with increase of temperature in summer. This dependence of the emanation of ^{222}Rn on meteorological conditions is not included in the TM3 model. The poor correspondence of the morning data is probably also caused by a bad representation of the night and morning ^{222}Rn profiles in the global model due to the large thickness of the lowest model layer (about 60 m), resulting in lower modelled ^{222}Rn concentrations under very stable meteorological conditions.

Although the observed morning peak concentration is quite different from the modelled morning concentration, the afternoon concentrations agree quite well with the observations (see Fig. 12). As for the ^{222}Rn concentrations in Freiburg, we see that the L6 scheme leads to the highest morning concentrations, while the E6 case gives the lowest values. The H3 case gives intermediate values.

Measurements of ^{222}Rn have been made at Socorro from November 1951 until June 1957. These data were used to generate monthly mean daily cycles of the ^{222}Rn concentration (Wilkening, 1959). We have compared the monthly mean daily cycles from January 1959 until February 1963 with these data. The result can be seen in Fig. 13. The afternoon values for E6, L6 and H3 are very similar. It shows that the E6 scheme reproduces these values best, while there is still some large deviation in the period 06:00–09:00 LT due to the time averaging in the E6 case. This also shows up in Table 6 where the correlation between the modelled and the observed ^{222}Rn concentration is given. In December and January, all schemes seem to fail in reproducing the low observed ^{222}Rn concentrations. This probably has to be attributed again to lower ^{222}Rn emissions in winter (soil-freezing). The mean values are given in Table 7.

ACPD
4, 4131–4189, 2004

3.4. Global ^{222}Rn distribution

In order to see the effect of diffusive transport on the free tropospheric concentrations of tracers, we now consider the budgets and transport of ^{222}Rn. The effect of diffusion in general is such that it leads to differences of up to 30% in the zonal mean ^{222}Rn concentration compared to the case where no diffusion is applied in the TM3 model. Smaller diffusion coefficients lead to higher ^{222}Rn concentration in the lowest layers and higher concentrations higher up in the atmosphere. The effect or influence of diffusion is strongest in the parts of the atmosphere with strong downward large scale motion like the subtropics, and/or where there is no vertical mixing by convection. In Fig. 14, the relative difference in ^{222}Rn concentrations between the E3 and H3 case and between the E3 and L6 case is shown for DJF 1993.

If we compare the E6 and E3 case, the zonal mean differences are everywhere smaller than 1% (not shown).

If we compare H3 and L6 with E3, we always see that the ^{222}Rn concentration in the lowest 500–1000 m is lower for E3, while above 1 km it is higher for E3. This higher concentration for H3 and L6 in the lowest layers of the atmosphere, leads to higher ^{222}Rn concentrations in the upper troposphere by convection, which transports the surface air to high altitudes in the tropics.

If we compare the H3 and E3 case, we see much higher concentrations in the E3 case in almost the whole troposphere (except the lowest layers). The stronger diffusion gives more mixing. Large differences can be found around 700 hPa in the winter subtropics, i.e. around 20° N in DJF and around 20° S in JJA (not shown).

If we compare L6 and E3, we see the effect of stronger diffusion and larger ABL heights in the winter subtropics. Through more intense and higher mixing, the ^{222}Rn concentrations are 5 to 10% higher around 500 hPa and 15% lower around 800 hPa in DJF around 20° N and in JJA around 20° S. In contrast to the general pattern mentioned before, we see in JJA around the North Pole higher concentrations in the lowest kilometer in the E6 case. Because there is almost no ^{222}Rn emission north of 60° N,

ACPD
4, 4131–4189, 2004

the concentration is higher in the free troposphere than at the surface (via long range transport). The increased mixing in the E3 case will then transport this ^{222}Rn downward.

This difference between the L6 and E3 concentration seems to contradict the mean diffusion profiles observed in Figs. 2 and 3. The mean L6 profiles are the result of very large diffusion coefficients during daytime, and small diffusion coefficients during nighttime. The ^{222}Rn transport or ^{222}Rn profile during daytime is not very sensitive to the exact values of the large diffusion coefficients during daytime. However the smaller diffusion coefficients during the night, lead to considerably higher night ^{222}Rn concentrations. The net effect is less diffusive upward transport.

Because ^{222}Rn has a short lifetime (about 5.5 days), we can deduce the global mean net vertical ^{222}Rn transport and changes therein due to differences in the diffusion schemes from its mean distribution. The net flux profile of ^{222}Rn is an indication of how the vertical diffusion will affect other tracers. This flux strongly depends on the source characteristics of the tracer (which are uniform on the continent for ^{222}Rn), and it is also strongly dependent on the sinks and the lifetime. It demonstrates the effect of different diffusion schemes on the tracer distribution.

In Fig. 15, we show the net global vertical ^{222}Rn fluxes. All fluxes are expressed relative to the E3-case. The differences in net global transport are maximally 4%. The difference is largest around 900 hPa. The difference between E3 and E6 are less than 1%. The net transport for the H3 case is stronger than the E3 case above 500 hPa, and stronger for the L6 case than the E3 case above 700 hPa. The interaction between the convection and the ABL turbulence is clearly visible. One can observe the following pattern: weaker transport in the lower troposphere leads to stronger transport in and into the upper troposphere. As mentioned before, if the turbulent transport is weaker, more ^{222}Rn remains in the lowest atmospheric levels, which can then be transported to the upper troposphere via fast convective transport. Higher concentrations at the surface (due to less turbulent transport) thus lead to higher concentrations in the upper troposphere.

ACPD
4, 4131–4189, 2004

In general, one can see in Fig. 15 that the differences in concentration and transport are quite small. This can partly be attributed to the fact that diffusion is not the only way of vertical transport. If the diffusive transport changes, it will be partly be compensated by convective or large scale vertical transport. The differences are also small because of time and spatial averaging.

4. Conclusions

We have studied the use of archived vertical diffusion coefficient from the ERA-40 project for making simulations with chemistry transport models. We compared 4 sets of vertical diffusion coefficients: (E3) 3-hourly archived coefficients based on a non-local scheme, (H3) 3-hourly off-line diagnosed coefficients based on a non-local scheme, (E6) as E3 but 6-hourly values, and (L6) 6-hourly off-line diagnosed coefficients based on a local diffusion scheme. We also compared the ABL height of the sets E6 and H3.

The off-line diagnosed set of non-local diffusion coefficients (H3) is based on a parameterisation that is very similar to the parameterisation used in the ECMWF model to generate the archived diffusion coefficients (E3/E6). We find that the results are quite similar between the E3 and H3 case (both with 3-hourly time resolution), and that the apparent difference can be attributed to differences in the parameterisation (different asymptotic mixing length, different stability functions, present or absent detrainment formulation). Hence the off-line diagnosis of diffusion coefficients reproduces quite well the archived diffusion coefficients. Also the off-line diagnosed ABL height corresponds well with the archived ABL height.

Comparison with ABL height measurements show that the ABL height archived in ERA-40 (E6) and the ABL height from the 3-hourly off-line non-local scheme (H3) are in good agreement with the ABL height observations performed in Cabauw and during the FIFE campaign. The time resolution of 3 h makes the H3 ABL height however more valuable than the 6-hourly E6 ABL height.

Comparison of ^{222}Rn simulations from the TM3 model with surface ^{222}Rn observa-

ACPD
4, 4131–4189, 2004

tions in Freiburg, Schauinsland, Cincinnati, and Socorro shows that the 3-hourly E3 and H3 schemes perform better than the 6-hourly E6 and L6 schemes. It also shows that using time-averaged diffusion coefficients can lead to larger timeshifts of the daily cycle of the ^{222}Rn concentration and stronger transport than using instantaneous diffusion coefficients.

Using 3-hourly E3 instead of 6-hourly E6 archived diffusion coefficients leads only to small differences in the mean ^{222}Rn concentration: using the 6-hourly coefficients causes slightly more diffusion. However, using the 3-hourly coefficients results in a better description of the daily cycle of the ^{222}Rn concentration. This might have an impact on tracers which undergo fast photochemistry or are affected by dry deposition or vegetation.

Although the mean values of the diffusion coefficients in the lower troposphere were larger for the L6 case than for the E6 case, the actual boundary layer transport was less. First, this could be attributed to the fact that the daytime ^{222}Rn concentrations are not very sensitive to the much larger daytime L6 diffusion coefficients, while the smaller nighttime diffusion coefficients have a strong impact on the night concentration. Secondly, the time averaging of the E6 coefficients instead of the instantaneous values of the L6 case causes more transport in the E6 than in the L6 case.

Using the E3 scheme results in higher ^{222}Rn concentrations in the free troposphere than using the H3 scheme. The seasonal zonal and monthly mean ^{222}Rn concentration can differ up to 10%. Earlier studies with the TM3 model suggested a too small vertical mixing. As mentioned before, this difference can be attributed to the use of the detrainment formulation at the top of the ABL for the E3 case, a larger asymptotic mixing length, and differences in the stability functions. It would be worthwhile making these changes in the H3-scheme. Also the influence of time-averaged versus instantaneous values could contribute to the differences.

The non-local schemes which are used here, do not contain a counter gradient term. Also here, it could be interesting to investigate whether including the counter-gradient term could further improve the agreement with measurements.

ACPD
4, 4131–4189, 2004

The ERA-40 data set starts in 1957. This allowed us to compare the simulated ^{222}Rn concentrations with ^{222}Rn observations made from 1959 until 1963. This makes the comparison to these observations more valuable than use in a climatological way. However, the difference between the modelled and measured morning concentration in Cincinnati are very large. The large discrepancy for this continental station suggests that a more physical based emanation rate of ^{222}Rn and maybe a higher spatial resolution should be used.

Finally, we recommend the use of 3-hourly archived vertical diffusion coefficients for ^{222}Rn simulation in chemistry transport modelling.

Acknowledgements. This evaluation of diffusion coefficients would not have been possible without the atmospheric monitoring work of H. Sartorius from the Federal Office for Radiation Protection in Freiburg, Germany, who provided ^{222}Rn data from the locations Freiburg and Schauinsland. We thank H. Klein Baltink for the ABL height measurement data from Cabauw. ECMWF ERA-40 data used in this study have been provided by ECMWF. This work was supported by the Netherlands Organization for Scientific Research (NWO) and by the European Union under contract number EVK2-CT-2002-00170 (RETRO).

References

Allen, D. J., Rood, R. B., Thompson, A. M., and Hudson, R. D.: Three-dimensional radon 222 calculations using assimilated meteorological data and a convective mixing algorithm, J. Geophys. Res., D3, 101, 6871–6881, 1996. 4134, 4135, 4141

Balkanski, Y. J. and Jacob, D. J.: Transport of continental air to the subantarctic Indian Ocean, Tellus B, 42, 62–75, 1990. 4141

Beljaars, A. C. M. and Viterbo, P.: Role of the boundary layer in a numerical weather prediction model, in Clear and cloudy boundary layers, edited by Holtslag, A. A. M. and Duynkerke, P. G., 287–304, NH-publishers, 1999. 4132, 4135, 4138, 4139

Bregman, B., Segers, A., Krol, M., Meijer, E., and van Velthoven, P.: On the use of mass-conserving wind fields in chemistry transport models, Atmos. Chem. Phys., 3, 447–457, 2003. 4143

Broecker, W. S., Li, Y. H., and Cromwell, J.: Radium-226 and radon-222 concentration in Atlantic and Pacific Oceans, Science, 158, 1307–1310, 1967. 4142

Brost, R. A. and Chatfield, R. B.: Transport of radon in a three-dimensional, subhemispheric model, J. Geophys. Res., 94, 5095–5119, 1989. 4141

Conen, F. and Robertson, L. B.: Latitudinal distribution of radon-222 flux from continents, Tellus B, 54, 127–133, 2002. 4142

Dentener, F., Feichter, J., and Jeuken, A.: Simulation of the transport of ^{222}Rn using on-line and off-line global models at different horizontal resolutions: a detailed comparison with measurements, Tellus B, 51, 573–602, 1999. 4135, 4141, 4142, 4147

Dentener, F., Peters, W., Krol, M., van Weele, M., Bergamaschi, P., and Lelieveld, J.: Interannual variability and trend of CH_4 lifetime as measure for OH changes in the 1979–1993 time period, J. Geophys. Res., 108, D11303, doi:10.1029/2002JD002916, 2003a. 4135, 4142

Dentener, F., van Weele, M., Krol, M., Houweling, S., and van Velthoven, P.: Trends and interannual variability of methane emissions derived from 1979–1993 global CTM simulations, Atmos. Chem. Phys, 3, 73–88, 2003b. 4142

Eloranta, E. W.: Boundary Layer Heights: LIDAR (FIFE), Data set., Available on-line (http://www.daac.ornl.gov) from Oak Ridge National Laboratory Distributed Active Archive Center, Oak Ridge, Tennessee, USA., also published in Strebel, D. E., Landis, D. R., Huemmrich, K. F., and Meeson, B. W. (Eds.), Collected Data of the First ISLSCP Field Experiment, Vol. 1: Surface Observations and Non-Image Data Sets, CD-ROM, National Aeronautics and Space Administration, Goddard Space Flight Center, Greenbelt, Maryland, USA, 1994. 4146

Feichter, J. and Crutzen, P. J.: Parameterization of vertical transport due to deep cumulus convection in a global transport model and its evaluation with ^{222}Radon measurements, Tellus B, 42, 100–117, 1990. 4135, 4141

Gold, S., Barkhau, H. W., Shleien, B., and Kahn, B.: Measurements of naturally occuring radionucleides in air, in The Natural Radiation Environment, edited by Adams, J. A. S. and Lowder, W. M., 369–382, University of Chicago Press, Chicago, Ill., 1964. 4152, 4153

Gregory, D., Morcrette, J.-J., Jakob, C., Beljaars, A. C. M., and Stockdale, T.: Revision of convection, radiation and cloud schemes in the ECMWF Integrated Forecasting System, Q. J. R. Meteor. Soc., 126, 1685–1710, 2000. 4143

Holtslag, A. A. M. and Boville, B. A.: Local versus nonlocal boundary-layer diffusion in a global climate model, J. Climate, 6, 1825–1842, 1993. 4132, 4134, 4135, 4137, 4139, 4140, 4141

Holtslag, A. A. M., van Meijgaard, E., and de Rooy, W. C.: A comparison of boundary layer

diffusion schemes in unstable conditions over land, Boundary-Layer Meteor., 76, 69–95, 1995. 4134

Houweling, A., Dentener, F., and Lelieveld, J.: The impact of nonmethane hydrocarbon compounds on tropospheric photochemistry, J. Geophys. Res., D9, 103, 10 673–10 696, 1998. 4142

Jacob, D. J. and Prather, M. J.: Radon-222 as a test of boundary layer convection in a general circulation model, Tellus B, 42, 117–134, 1990. 4135, 4141

Jacob, D. J., Prather, M. J., Rasch, P. J., Shia, R.-L., Balkanski, Y. L., Beagley, S. R., Bergmann, D. J., Blackshear, W. T., Brown, M., Chiba, M., Chipperfield, M. P., de Grandpré, J., Dignon, J. E., Feichter, J., Genthon, C., Grose, W. L., Kasibhatla, P. S., Köhler, I., Kritz, M. A., Law, K., Penner, J. E., Reeves, M. R. C. E., Rotman, D. A., Stockwell, D. Z., van Velthoven, P. F. J., Verver, G., Wild, O., Yang, H., and Zimmerman, P.: Evaluation and intercomparison of global transport models using ^{222}Rn and other short-lived tracers, J. Geophys. Res., D5, 102, 5953–5970, 1997. 4135, 4142

Jeuken, A.: Evaluation of chemistry and climate models using measurements and data assimilation, Ph.D. thesis, University of Technology Eindhoven, Eindhoven, The Netherlands, available at http://alexandria.tue.nl/extra2/200001283.pdf, 2000. 4139

Jeuken, A., Veefkind, J. P., Dentener, F., Metzger, S., and Gonzales, C. R.: Simulation of the aerosol optical depth over Europe for August 1997 and a comparison with observations, J. Geophys. Res., D22, 106, 28 295–28 311, 2001. 4139

Kritz, M. A., Roulley, J.-C. L., and Danielsen, E. F.: The China Clipper – fast advective transport of radon-rich air from the Asian boundary layer to the upper troposphere near California, Tellus B, 42, 46–61, 1990. 4141

Lambert, G., Polian, G., Sanak, J., Ardouin, B., Buisson, A., Jegou, A., and Roulley, J. C. L.: Cycle du radon et de ses descendants: application à l'étude des échanges troposphère-stratosphère, Ann. Géophys., 4, 38, 497–531, 1982. 4142

Lee, H. N. and Larsen, R. J.: Vertical diffusion in the lower atmosphere using aircraft measurements of ^{222}Rn, J. Appl. Meteorol., 36, 1262–1270, 1997. 4135

Lelieveld, J. and Dentener, F.: What controls tropospheric ozone?, J. Geophys. Res., D3, 105, 3531–3551, 2000. 4142

Liu, S. C., McAfee, J. R., and Cicerone, R. J.: Radon 222 and tropospheric vertical transport, J. Geophys. Res., D5, 7291–7297, 1984. 4142

Louis, J.-F.: A parametric model of vertical eddy fluxes in the atmosphere, Bound.-Layer Me-

teor., 17, 187–202, 1979. 4132, 4133, 4135, 4140, 4141
Louis, J. F., Tiedtke, M., and Geleyn, J. F.: A short history of the operational PBL-parameterization at ECMWF, in Proceedings of ECMWF workshop on boundary layer parameterization, November 1981, 59–79, ECMWF, Reading, England, 1982. 4132, 4135, 4138, 4141
Mahowald, N. M., Rasch, P. J., Eaton, B. E., Whittlestone, S., and Prinn, R.: Transport of ^{222}radon to the remote troposphere using the Model of Atmospheric Transport and Chemistry and assimilated winds from ECMWF and the National Center for Environmental Prediction/NCAR, J. Geophys. Res., D23, 102, 28 139–28 151, 1997. 4135
Meijer, E. W., van Velthoven, P. F. J., Thompson, A. M., Pfister, L., Schlager, H., Schulte, P., and Kelder, H.: Model calculations of the impact of NO_x from air traffic, lightning, and surface emissions, compared with measurements, J. Geophys. Res., D3, 105, 3833–3850, 2000. 4142
Nordeng, T. E.: Extended versions of the convective parametrization scheme at ECMWF and their impact on the mean and transient activity of the model in the tropics, Research Department Technical Memorandum 206, ECMWF, Reading RG2 9AX, UK, 1994. 4143
Olivié, D. J. L., van Velthoven, P. F. J., Beljaars, A., and Kelder, H. M.: Comparison between archived and off-line diagnosed convective mass fluxes in the chemistry transport model TM3, J. Geophys. Res., D11, 109, D11303, doi:10.1029/2003JD004036, 2004. 4143
Polian, G., Lambert, G., Ardouin, B., and Jegou, A.: Long-range transport of radon in subantarctic and antarctic areas, Tellus B, 38, 178–189, 1986. 4141
Rasch, P. J., Mahowald, N. M., and Eaton, B. E.: Representations of transport, convection, and the hydrological cycle in chemical transport models: Implications for the modeling of short-lived and soluble species, J. Geophys. Res., D23, 102, 28 127–28 138, 1997. 4134
Russell, G. L. and Lerner, J. A.: A new finite-differencing scheme for the tracer transport equation, J. Appl. Meteorol., 20, 1483–1498, 1981. 4143
Sellers, P. J., Hall, F. G., Asrar, G., Strebel, D. E., and Murphy, R. E.: The First ISLSCP Field Experiment (FIFE), Bull. Am. Meteor. Soc., 69, 22–27, 1988. 4145
Simmons, A. J. and Burridge, D. M.: An energy and angular-momentum conserving vertical finite-difference scheme and hybrid vertical coordinates, Mon. Weather Rev., 109, 758–766, 1981. 4143
Simmons, A. J. and Gibson, J. K.: The ERA-40 project plan, ERA-40 Project Report Series 1, ECMWF, Reading RG2 9AX, UK, 2000. 4135

Stockwell, D. Z. and Chipperfield, M. P.: A tropospheric chemical-transport model: development and validation of the model transport schemes, Q. J. R. Meteorol. Soc., 125, 1747–1783, 1999. 4135

Stockwell, D. Z., Kritz, M., Chipperfield, M. P., and Pyle, J. A.: Validation of an off-line three-dimensional chemical transport model using observed radon profiles 2. Model results, J. Geophys. Res., D7, 103, 8433–8445, 1998. 4135

Tiedtke, M.: A comprehensive mass flux scheme for cumulus parameterization in large-scale models, Mon. Weather Rev., 117, 1779–1800, 1989. 4143

Troen, I. and Mahrt, L.: A simple model of the atmospheric boundary layer; sensitivity to surface evaporation, Bound.-Layer Meteor., 37, 129–148, 1986. 4133, 4137, 4139

Turekian, K. K., Nozaki, Y., and Benninger, L. K.: Geochemistry of atmospheric radon and radon products, Ann. Rev. Earth Planet. Sci., 5, 227–255, 1977. 4142

van Velthoven, P. F. J. and Kelder, H.: Estimates of stratosphere-troposphere exchange: Sensitivity to model formulation and horizontal resolution, J. Geophys. Res., D1, 101, 1429–1434, 1996. 4142

Viterbo, P., Beljaars, A., Mahfouf, J.-F., and Teixeira, J.: The representation of soil moisture freezing and its impact on the stable boundary layer, Q. J. R. Meteor. Soc., 125, 2401–2426, 1999. 4139

Vogelezang, D. H. P. and Holtslag, A. A. M.: Evaluation and model impacts of alternative boundary-layer height formulations, Bound.-Layer Meteor., 81, 245–269, 1996. 4132, 4135, 4139, 4140

Wang, K.-Y., Pyle, J. A., Sanderson, M. G., and Bridgeman, C.: Implementation of a convective atmospheric boundary layer scheme in a tropospheric chemistry transport model, J. Geophys. Res., D19, 104, 23 729–23 745, 1999. 4133, 4134, 4141

Wilkening, M. H.: Daily and annual courses of natural atmospheric radioactivity, J. Geophys. Res., 64, 521–526, 1959. 4152, 4153

Wilkening, M. H. and Clements, W. E.: Radon 222 from the ocean surface, J. Geophys. Res., 80, 3828–3830, 1975. 4142

Williamson, D. L., Kiehl, J. T., Ramanathan, V., Dickinson, R. E., and Hack, J. J.: Description of NCAR Community Climate Model (CCM1), NCAR Technical Note 285, NCAR, 1987. 4140

Table 1. Overview of the diffusion schemes.

code	scheme	timestep	data origin	K_h	ABL height
E3	non-local	3 h	archived	averaged	
H3	non-local	3 h	off-line diagnosed	instantaneous	instantaneous
E6	non-local	6 h	archived	averaged	instantaneous
L6	local	6 h	off-line diagnosed	instantaneous	
N	no diffusion				

ACPD
4, 4131–4189, 2004

Table 2. Correlation of the observed with the modelled ABL height during the FIFE campaign and in Cabauw.

diffusion	FIFE campaign (N=187)	Cabauw (N=437)
H3	0.835	0.845
E6	0.755	0.755

ACPD
4, 4131–4189, 2004

Table 3. Mean value of the ^{222}Rn concentration in 1993 in Freiburg and Schauinsland. The ^{222}Rn concentration is expressed in 10^{-21} mol mol^{-1}.

diffusion	Freiburg	Schauinsland
E3	102±45	43±18
H3	110±59	43±19
E6	98±41	43±18
L6	125±68	42±18
N	501±113	31±21
observed	113±70	37±19

ACPD
4, 4131–4189, 2004

Table 4. Correlation of the modelled with the observed ^{222}Rn concentration in 1993 in Freiburg and Schauinsland. In column (a) the correlation of the modelled with the observed daily mean is given, in column (b) the correlation of the modelled with the observed hourly value, and in column (c) the correlation of the modelled with the observed deviation from the mean daily value.

diffusion	Freiburg			Schauinsland		
	(a) (N=306)	(b) (N=7731)	(c) (N=7344)	(a) (N=243)	(b) (N=7250)	(c) (N=5832)
E3	0.870	0.773	0.498	0.649	0.563	0.276
H3	0.871	0.790	0.522	0.644	0.537	0.231
E6	0.871	0.759	0.449	0.654	0.558	0.227
L6	0.844	0.735	0.484	0.669	0.565	0.283
N	0.704	0.648	0.364	0.469	0.382	0.134

ACPD
4, 4131–4189, 2004

Table 5. Correlation between the observed and modelled ratio of the ^{222}Rn concentration in Freiburg and in Schauinsland in 1993.

diffusion	Freiburg/Schauinsland (N=6531)
E3	0.735
H3	0.769
E6	0.712
L6	0.705
N	0.570

ACPD
4, 4131–4189, 2004

Table 6. Correlation of the observed with the modelled ^{222}Rn concentration in Cincinnati and Socorro.

diffusion	Cincinnati		Socorro
	morning (N=48)	afternoon (N=48)	daily cycle (N=288)
H3	0.523	0.388	0.823
E6	0.639	0.399	0.714
L6	0.711	0.421	0.759

ACPD
4, 4131–4189, 2004

Table 7. Mean observed and modelled ^{222}Rn concentrations at Socorro. The observations have been made between November 1951 and June 1957. The modelled concentrations are mean values for the period January 1959 until December 1962. The ^{222}Rn concentration is expressed in 10^{-21} mol mol^{-1}.

diffusion	Socorro
H3	113±44
E6	91±44
L6	121±44
observed	158

ACPD
4, 4131–4189, 2004

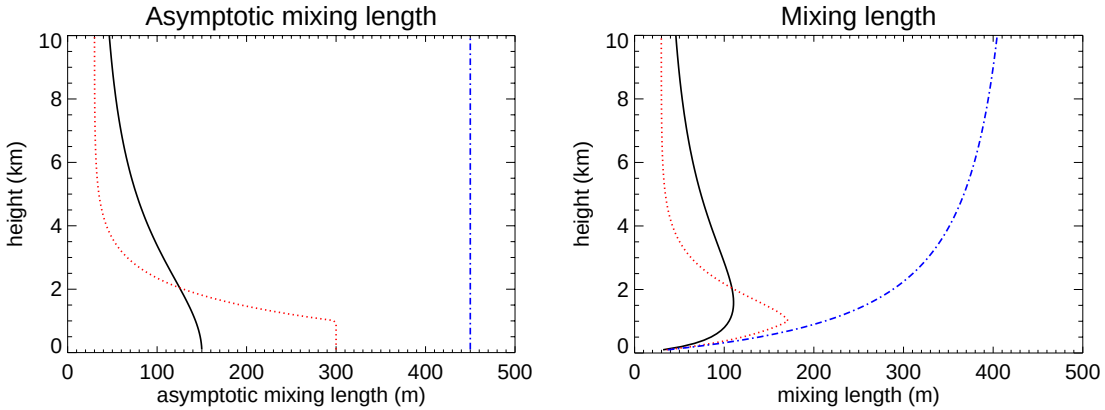

Fig. 1. Vertical profiles of the asymptotic mixing length (left) and mixing length (right) for heat in the different diffusion schemes: E3/E6 scheme (solid black line), H3 scheme (dotted red line), and L6 scheme (dot-dashed blue line). The mixing length can be derived from the asymptotic mixing length using Eq. (9).

ACPD
4, 4131–4189, 2004

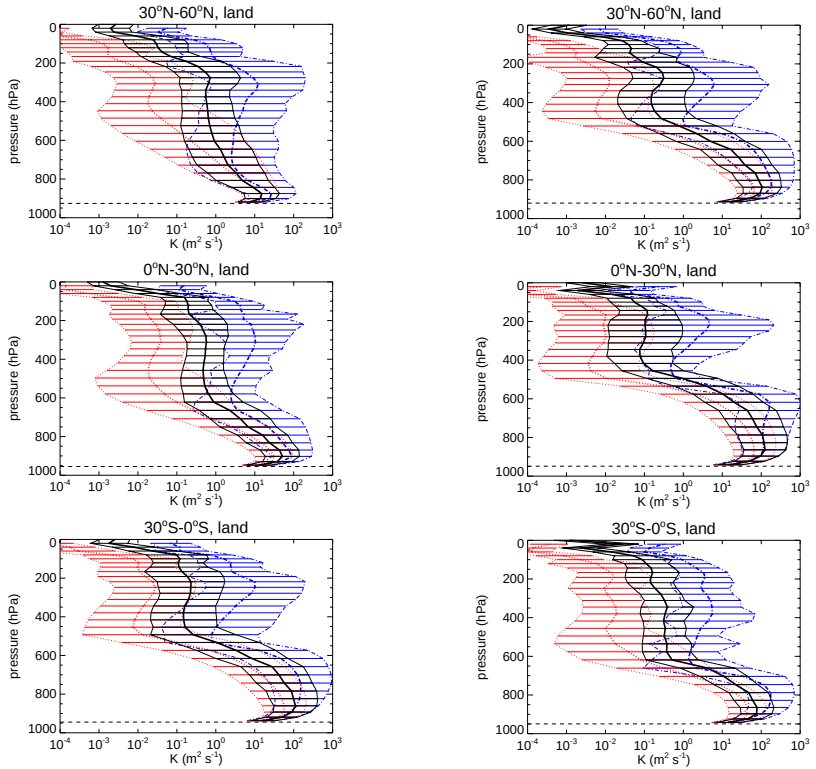

Fig. 2. Zonal and monthly mean profiles of the vertical diffusion coefficient for heat in January (left) and July (right) 1993 over land as a function of pressure level. Profiles are given separately for 3 latitude bands. The solid black line denotes the E3/E6 case, the dotted red line the H3 case, and the dot-dashed blue line the L6 case. The thick lines denote the mean value, the thin lines denote the 1σ standard deviation. The mean surface pressure level is indicated as the horizontal dashed line. For an overview of the different cases, see Table 1.

ACPD
4, 4131–4189, 2004

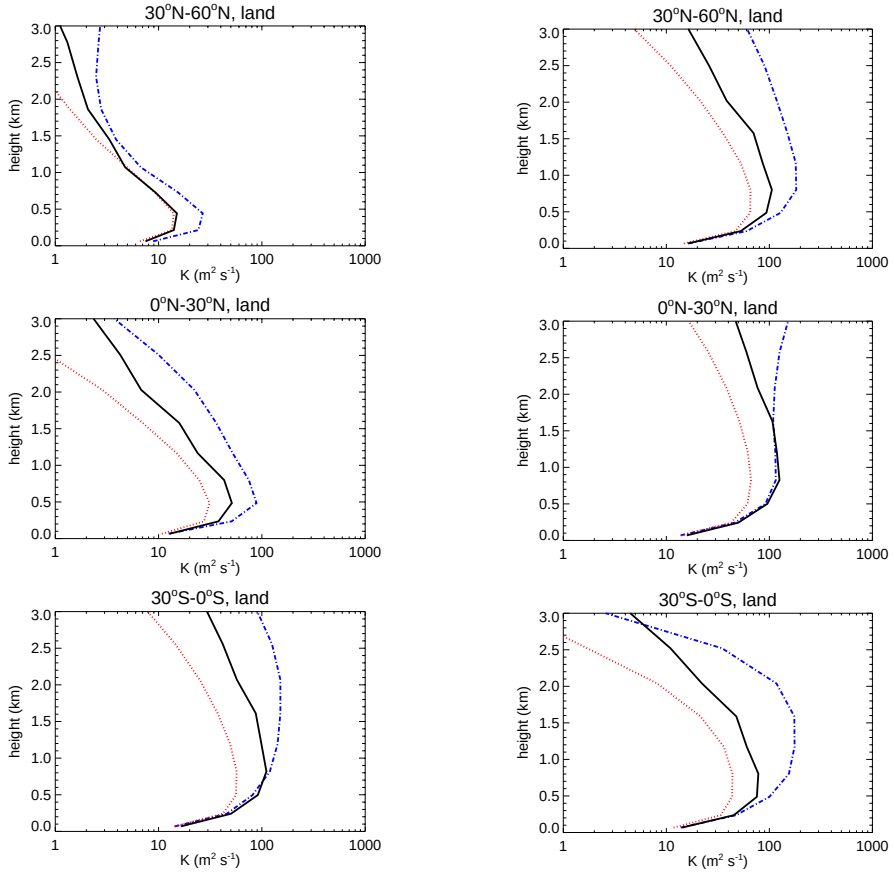

Fig. 3. As Fig. 2, but now with the height above the surface as the vertical coordinate.

ACPD
4, 4131–4189, 2004

Vertical diffusion coefficients from ERA-40

D. J. L. Olivié et al.

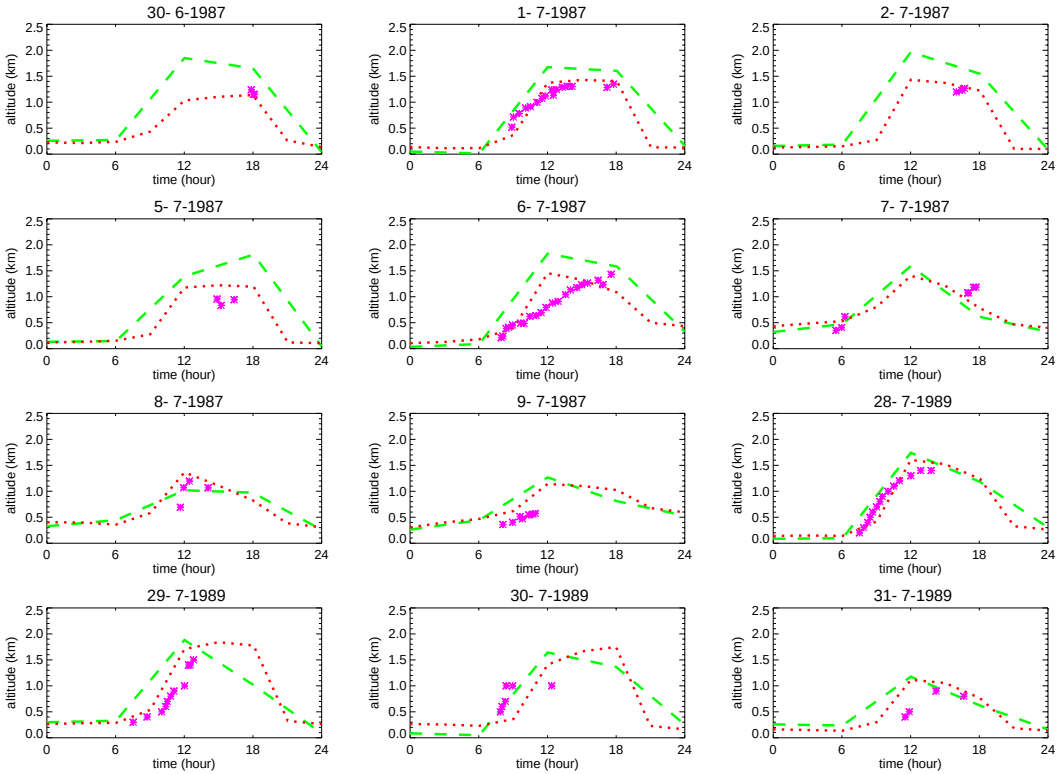

Fig. 4. Time evolution of the ABL height during the FIFE campaign in 1987 and 1989 in the US. Pink stars denote the observed ABL height, the dashed green line denotes the ABL height archived in the ERA-40 data (E6), the dotted red line denotes the ABL height calculated in the H3-scheme. The time is expressed in GMT−6 h.

ACPD
4, 4131–4189, 2004

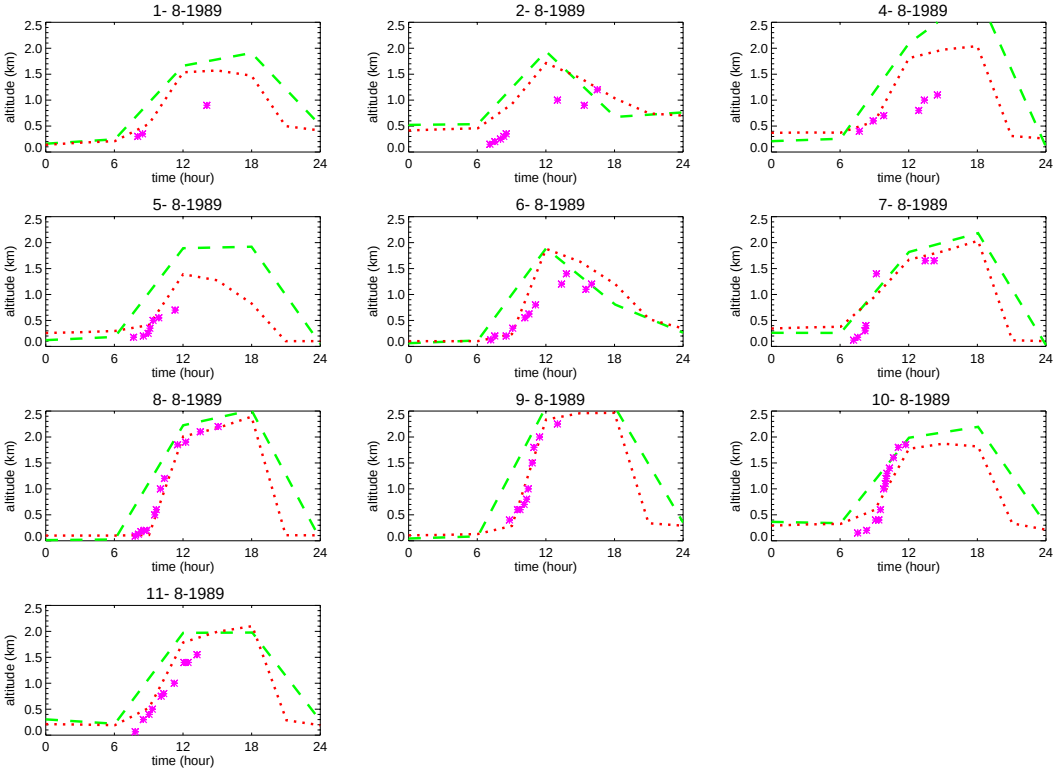

Fig. 4. Continued.

ACPD
4, 4131–4189, 2004

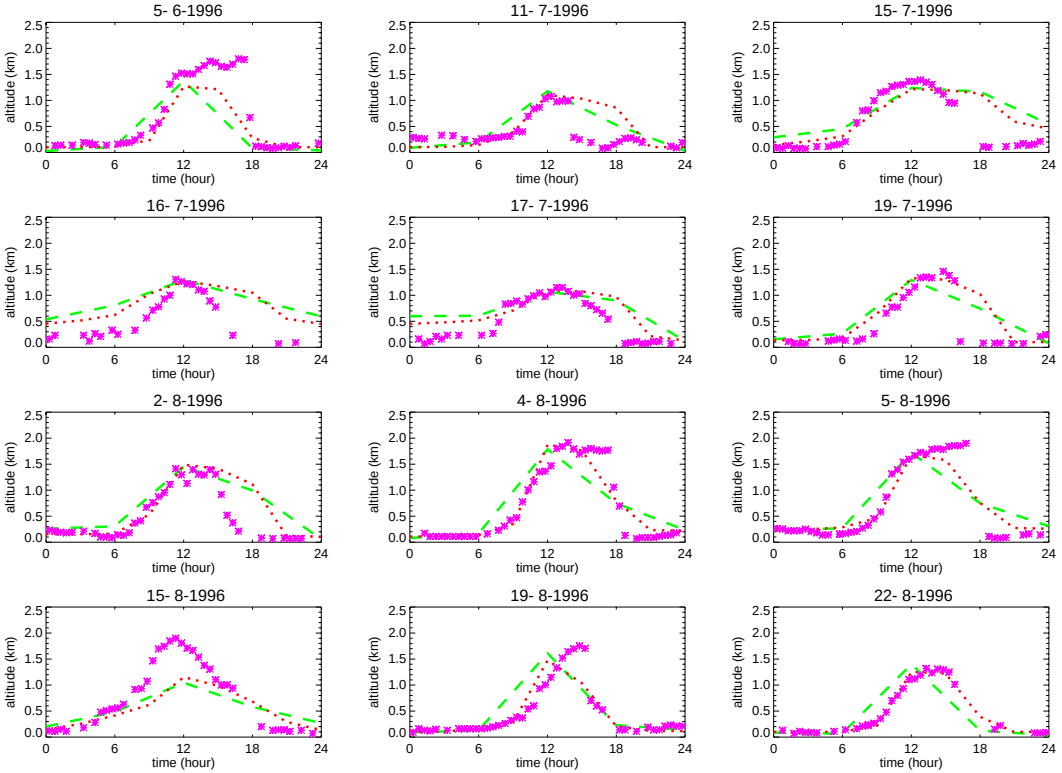

Fig. 5. Time evolution of the ABL height during some days in June, July and August 1996 in Cabauw, the Netherlands. Symbol and line code as in Fig. 4. The time is expressed in GMT.

ACPD
4, 4131–4189, 2004

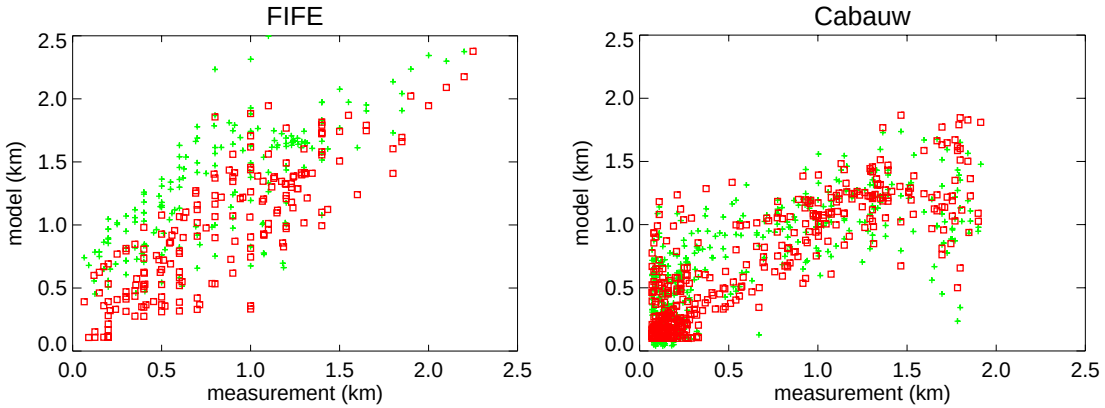

Fig. 6. Scatter plot of the ABL height during the FIFE campaign (left) and in Cabauw (right). Green crosses denote comparisons with the ERA-40 ABL height (E6), red squares denote comparisons with the ABL heights from the H3 scheme.

ACPD
4, 4131–4189, 2004

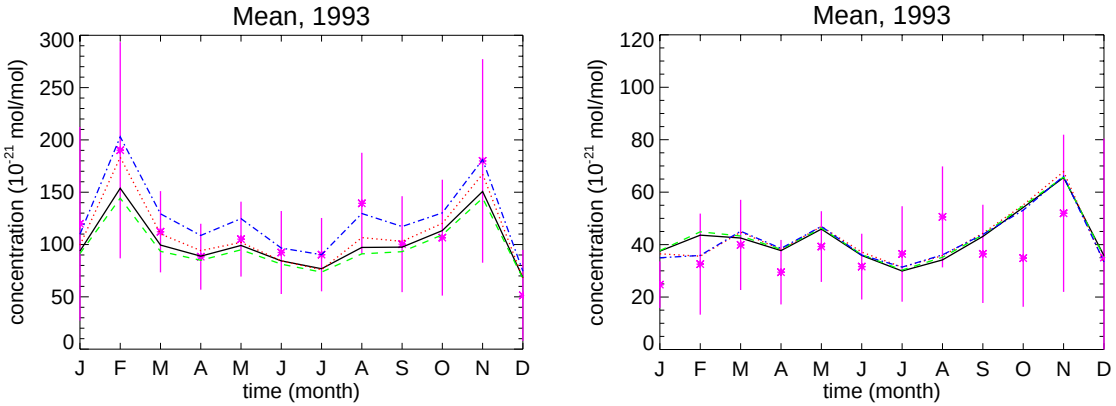

Fig. 7. Monthly mean ^{222}Rn concentration (upper panels), correlation of the modelled with the observed mean daily value (middle panels), and correlation of the observed with the modelled deviation of the hourly value from the daily mean value (lower panels), for Freiburg (left) and Schauinsland (right) in 1993. The pink stars denote the mean observations, the lines denote the results from the model runs: using E3 data (solid black line), using H3 data (dotted red line), using E6 data (dashed green line), and using L6 data (dot-dashed blue line). The error bars (upper panels) show the 1σ standard deviation of the observations.

ACPD
4, 4131–4189, 2004

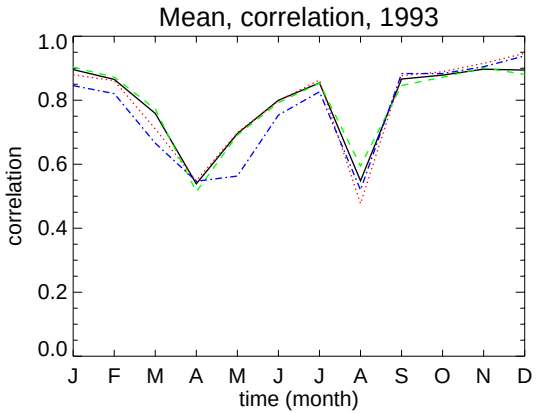

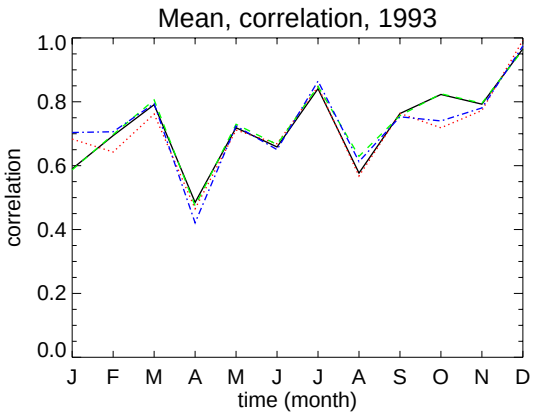

Fig. 7. Continued.

ACPD
4, 4131–4189, 2004

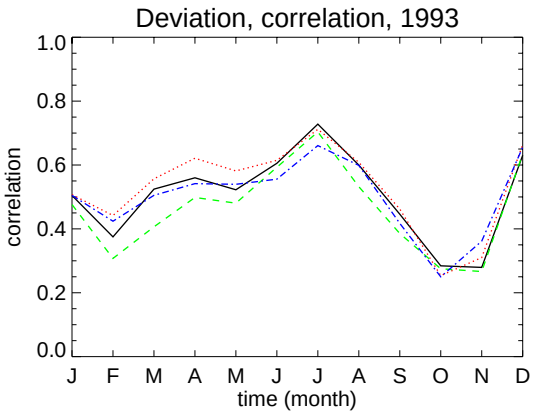

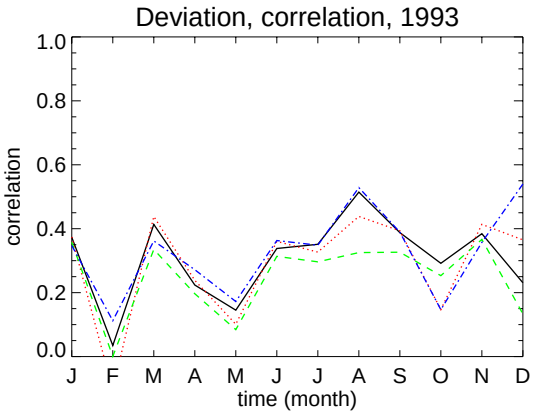

Fig. 7. Continued.

ACPD
4, 4131–4189, 2004

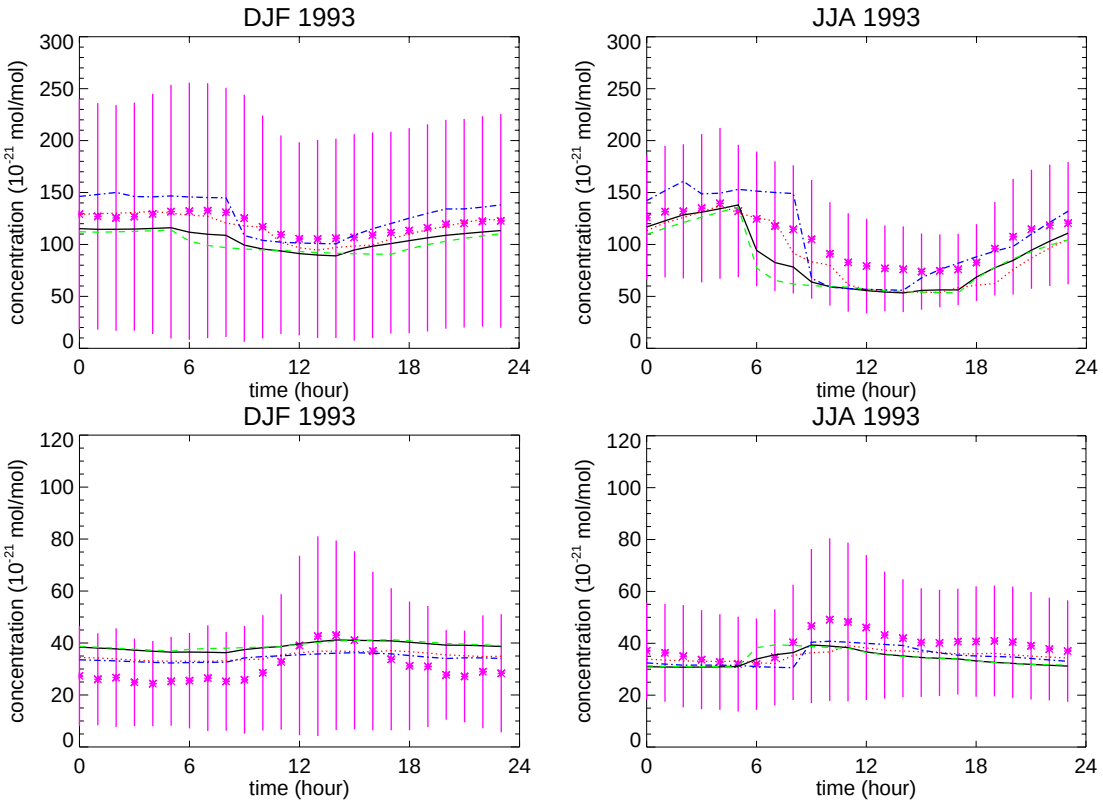

Fig. 8. Daily cycle of observed and modelled ^{222}Rn concentration in Freiburg in DJF (upper left) and JJA (upper right) and in Schauinsland in DJF (lower left) and JJA (lower right) 1993. The stars denote the observed value, the lines denote the modelled values (line code is as in Fig. 7). The error bars show the 1σ standard deviation of the observations.

ACPD
4, 4131–4189, 2004

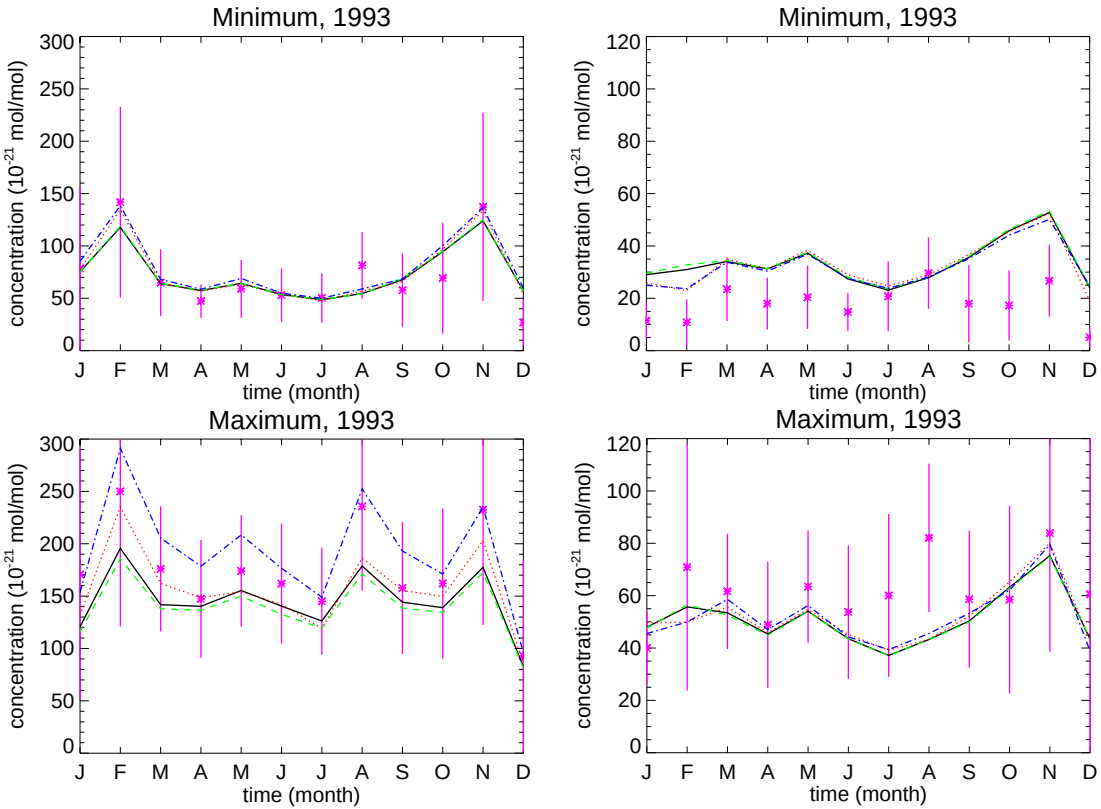

Fig. 9. Monthly mean of the daily minimum (upper panels), daily maximum (middle panels) and daily amplitude (lower panels) in the ^{222}Rn concentration in Freiburg (left) and Schauinsland (right) in 1993. The stars denote the measurements, the lines denote the results from the model runs (line code as in Fig. 7). The error bars show the 1σ standard deviation of the observations.

ACPD
4, 4131–4189, 2004

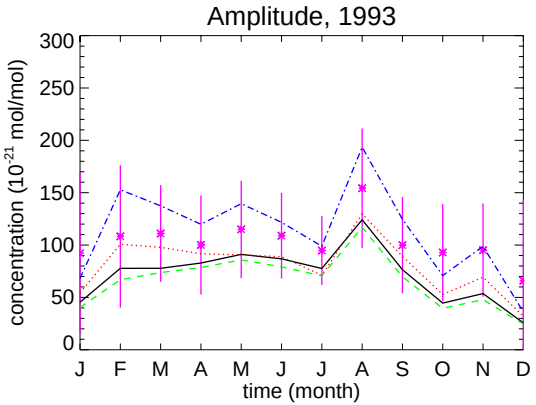

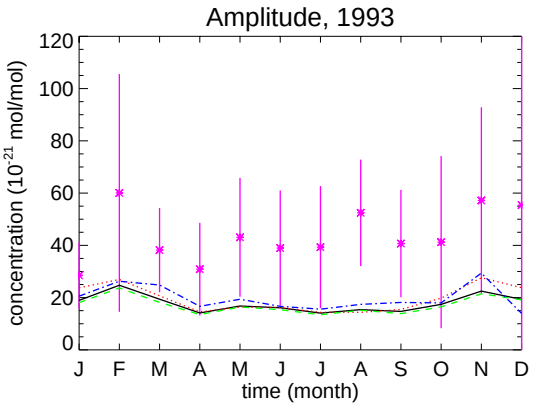

Fig. 9. Continued.

ACPD
4, 4131–4189, 2004

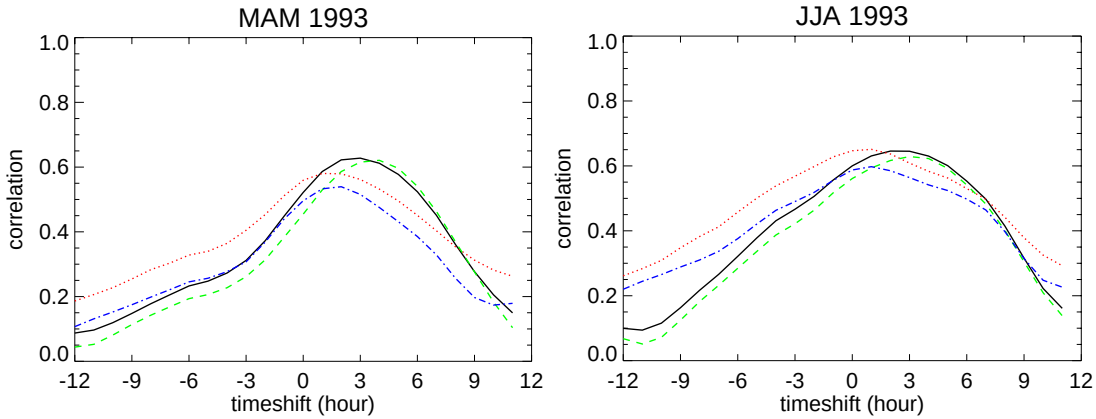

Fig. 10. The correlation of the hourly modelled with the hourly observed ^{222}Rn concentration in Freiburg in MAM (left) and JJA (right) as a function of the timeshift. Only the modelled concentration between 00:00 and 12:00 GMT is used. Values in the right hand part of the figure (positive timeshifts) give the correlation of model concentrations with a later observation, values in the left part of the figure (negative timeshifts) give the correlation of model concentrations with an earlier observation. Line code: using E3 data (solid black line), using H3 data (dotted red line), using E6 data (dashed green line), and using L6 data (dot-dashed blue line).

ACPD
4, 4131–4189, 2004

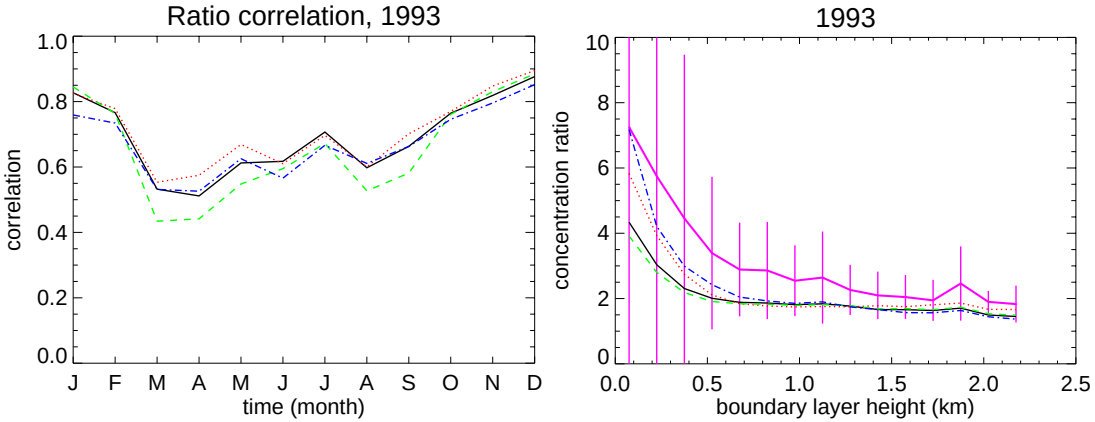

Fig. 11. Left panel: correlation of the modelled with the observed ratio of the concentration in Freiburg and the concentration in Schauinsland. Right panel: mean ratio between the ^{222}Rn concentration in Freiburg and the concentration in Schauinsland as a function of the ABL height (calculated with the H3 scheme) for the year 1993. The thick pink line denotes the ratio derived from the observed concentrations, the other lines denote the ratio's derived from the modelled concentrations using E3 data (solid black line), using H3 data (dotted red line), using E6 data (dashed green line), and using L6 data (dot-dashed blue line). To calculate these curves, we binned all the hourly ABL height data in 15 bins with a width of 150 m, ranging from 0 up to 2250 m. The ABL height is taken from the H3 scheme. The error bars denote the 1σ standard deviation of the ratio derived from the observed concentrations.

ACPD
4, 4131–4189, 2004

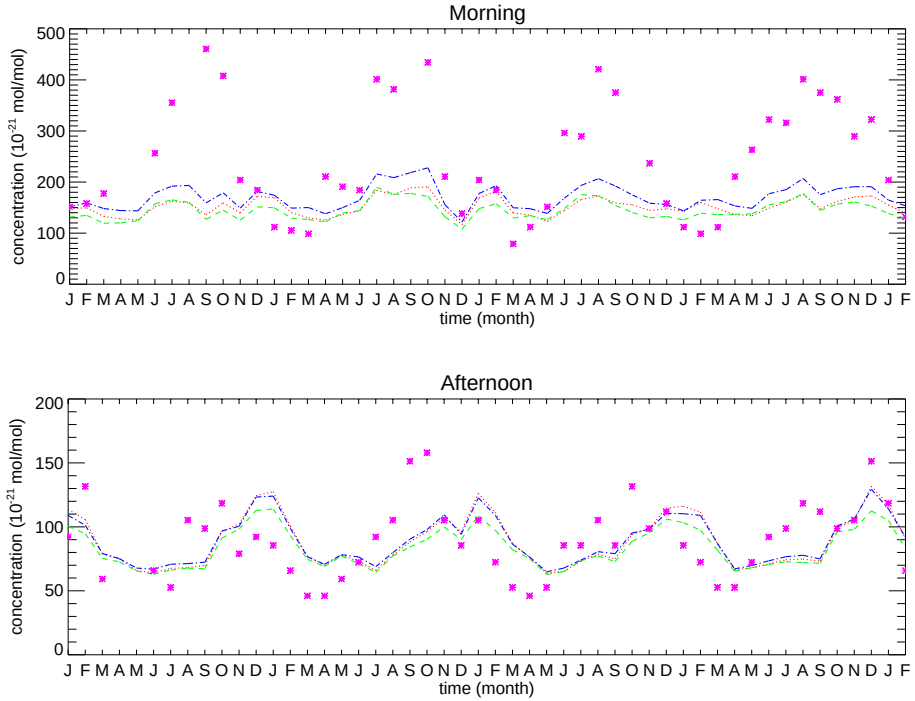

Fig. 12. Monthly mean morning (upper panel) and afternoon (middle panel) ^{222}Rn concentration from January 1959 until February 1963 at Cincinnati. Observed concentrations (pink stars) and modelled concentrations using H3 data (dotted red line), E6 data (dashed green line), and L6 (dot-dashed blue line) are shown. Scatterplots of the monthly mean morning (lower left) and afternoon (lower right) ^{222}Rn concentration are shown using H3 data (red triangles), using E6 data (green squares), and using L6 data (blue diamonds).

ACPD
4, 4131–4189, 2004

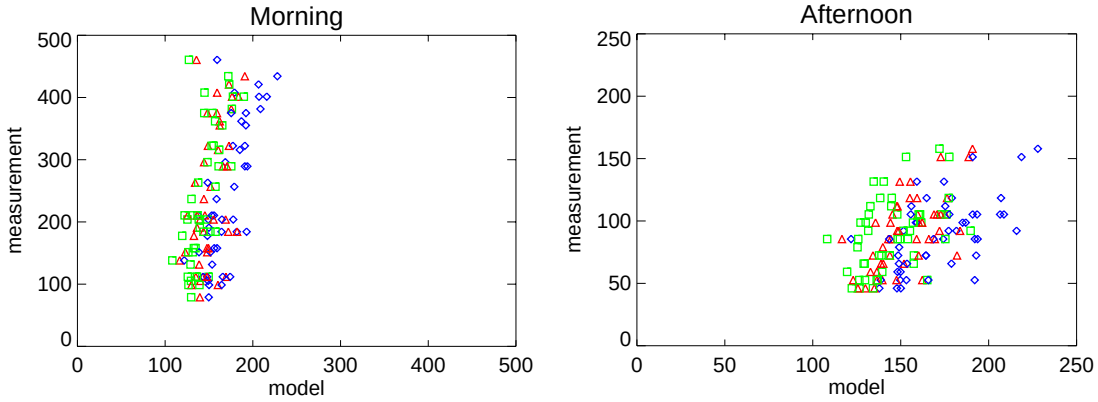

Fig. 12. Continued.

ACPD
4, 4131–4189, 2004

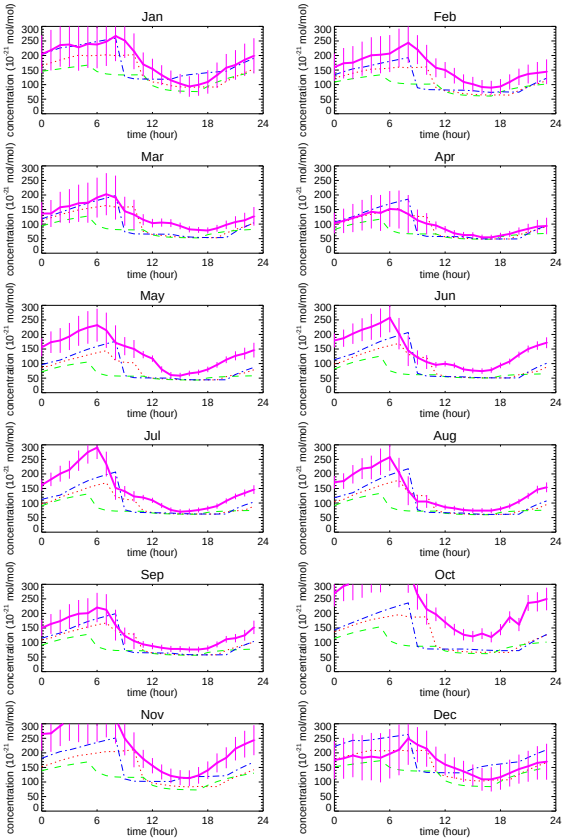

Fig. 13. Monthly mean daily cycle of ^{222}Rn concentration from January 1959 until February 1963 in Socorro: measured (thick solid pink line) and modelled using H3 (dotted red line), using E6 (dashed green line) and using L6 (dot-dashed blue line). The observed monthly mean daily cycles are based on measurements from November 1951 until June 1957. The error bars denote the 1σ standard deviation of the modelled concentration.

ACPD
4, 4131–4189, 2004

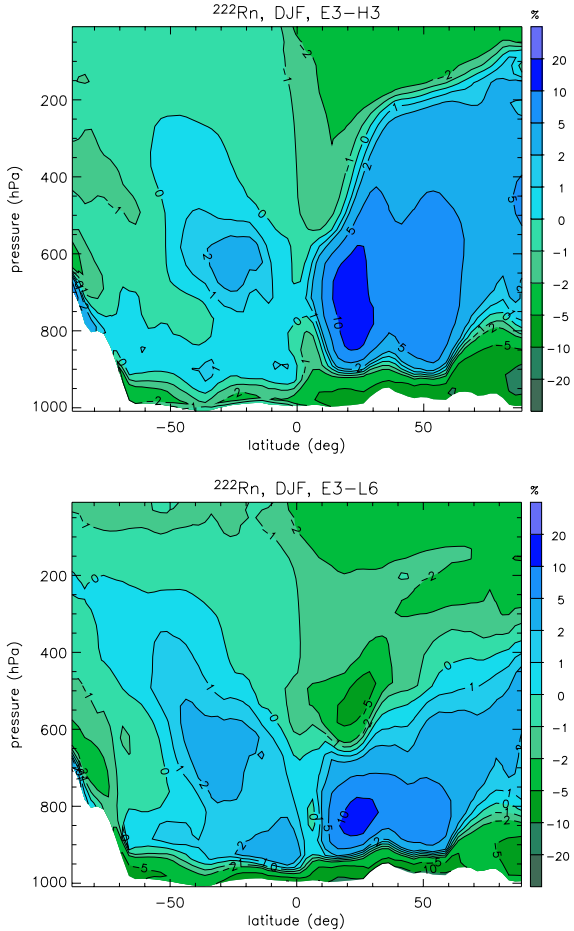

Fig. 14. Zonal mean relative difference (%) in ^{222}Rn concentration between E3 and H3 (upper panel) and between E3 and L6 (lower panel) for DJF 1993.

ACPD
4, 4131–4189, 2004

Vertical diffusion coefficients from ERA-40

D. J. L. Olivié et al.

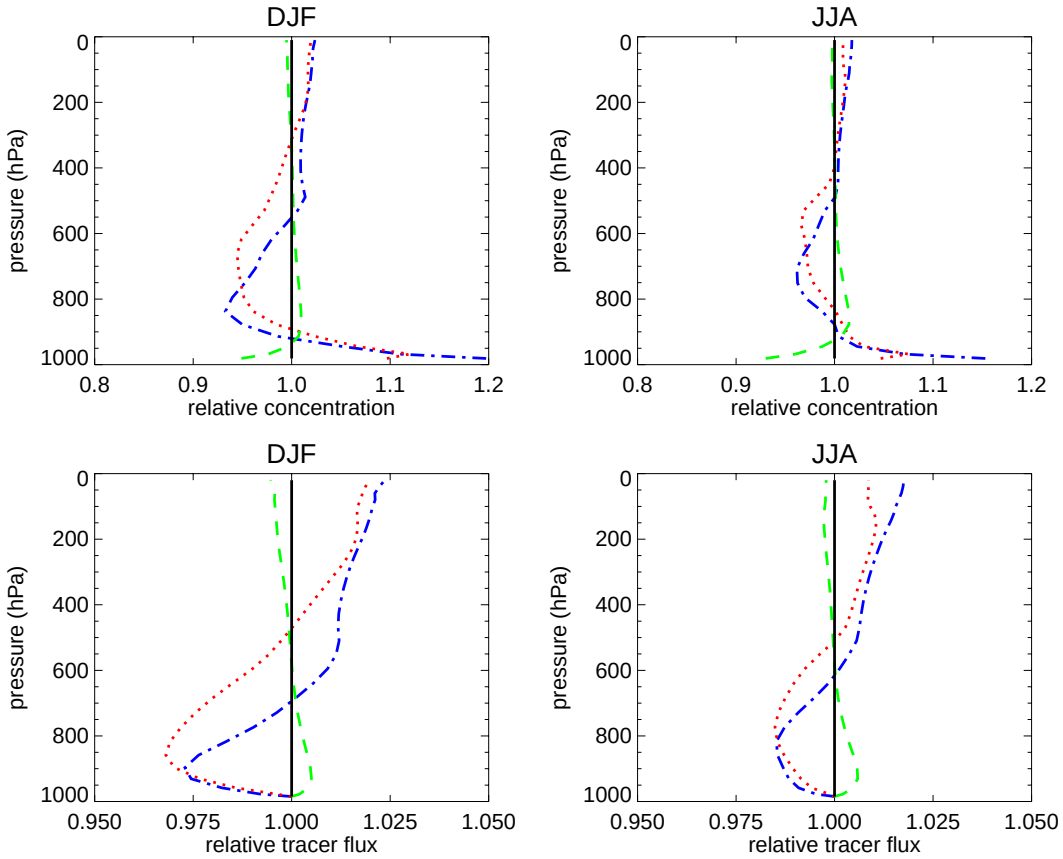

Fig. 15. Profiles of the global mean ^{222}Rn concentration (upper panels) and profiles of the global mean net upward ^{222}Rn flux (lower panels) are shown for DJF and JJA 1993. The concentration and flux of E3 (solid black), H3 (dotted red), E6 (dashed green), L6 (dot-dashed blue) are expressed with respect to the flux of E3.

ACPD
4, 4131–4189, 2004

Vertical diffusion coefficients from ERA-40

D. J. L. Olivié et al.